THESIS

MECHANICS OF EXTENDABLE WIND TURBINE BLADES

Submitted by

Jeswin John

Department of Civil and Environmental Engineering

In partial fulfillment of the requirements

For the Degree of Master of Science

Colorado State University

Fort Collins, Colorado

Spring 2015

Master's Committee:

Advisor: Paul Heyliger

Rebecca Atadero
Donald Radford

ABSTRACT

MECHANICS OF EXTENDABLE WIND TURBINE BLADES

This research aims at understanding the reductions in deflection, stress, and natural frequency of extendable wind turbine blades. For that purpose, a comparative study of these properties for the extendable turbine blade compared with those of a conventional turbine blade was completed. Wind turbine blades have seen extensive growth in application, and extendable turbine blades are a novel advancement over conventional blades. They can be more efficient in extracting energy from wind and are much more practical for transportation purposes. Lengths of the turbine blade have been increasing every year, and the next logical step is to consider making them extendable.

In this research, a basic model of the blade was created and then a three-dimensional linear elasticity model was used and studied using the finite element method for analyzing the crucial parameters. In addition to this, two different load cases and six different retracted blade positions were analyzed for in-depth study of the blade behavior. As far as loading is considered, an initial analysis was completed using the wind load alone to give a basic idea of how the model behaves under standard parked conditions. In the second case, both wind and dead load were considered to help understand the blade behavior from a more practical perspective. Overall, the research gives estimates of the reductions in stress, displacement, and natural frequency when the blades are extendable and gives better understanding into the design parameters of these novel structures.

TABLE OF CONTENTS

LIST OF TABLES

LIST OF FIGURES

CHAPTER 1: INTRODUCTION

In the modern world the demand for energy is increasing. Future demands would be far more secure if there was a robust means of harvesting renewable energy sources. Wind power is one of the most practical of these options. A typical arrangement to extract wind power is the use of wind turbines to convert the incident wind energy into usable electricity. Although based with their own challenges, they do not pollute or leave residual waste like most common non-renewable energy sources such as petroleum, coal or nuclear energy.

There are some major issues that concern this technology. The setup for a wind turbine consists of the tower, generator, transmission shaft, rotor and the turbine blades. The blades serve as the nexus between the wind and its conversion from kinetic energy into electric energy. Typically wind turbine blades are over 30 m long and are usually transported on roads or rail lines to reach their final constriction site. Hence it can be extremely challenging to maneuver trucks to get the blades from manufacturing factory to site of assembly without any damage. Since it is a costly affair to manufacture and transport the blade, it is not an option to deliver damaged blades.

Another concern in blade design is their efficiency. By the Betz Law the maximum efficiency possible for a wind turbine blade is about 52% [1]. A practical solution to these issues is the use of the extendable blades instead of conventional turbine blades. Extendable blades are basically what its name implies: they can be extended (or retracted) to a more optimal length similar to working of an Extendable Utility Knife. Figures 1.1 and 1.2 are some basic sketches of extendable blades, to help understand its geometry. Figure 1.2 is a modelled sketch of Blade 7, which is one of the retracted blade configurations considered for analysis in this study (All blade configurations are explained in Section 3.5 of Chapter 3). It consists of two blades, the root blade and the tip blade [1]. Its potential is enormous from enabling easier ways of transporting to the site due to its reduced length to providing higher power output. In this paper several basic mechanics parameters are studied to help understand its behavior in comparison to conventional wind turbine blades.

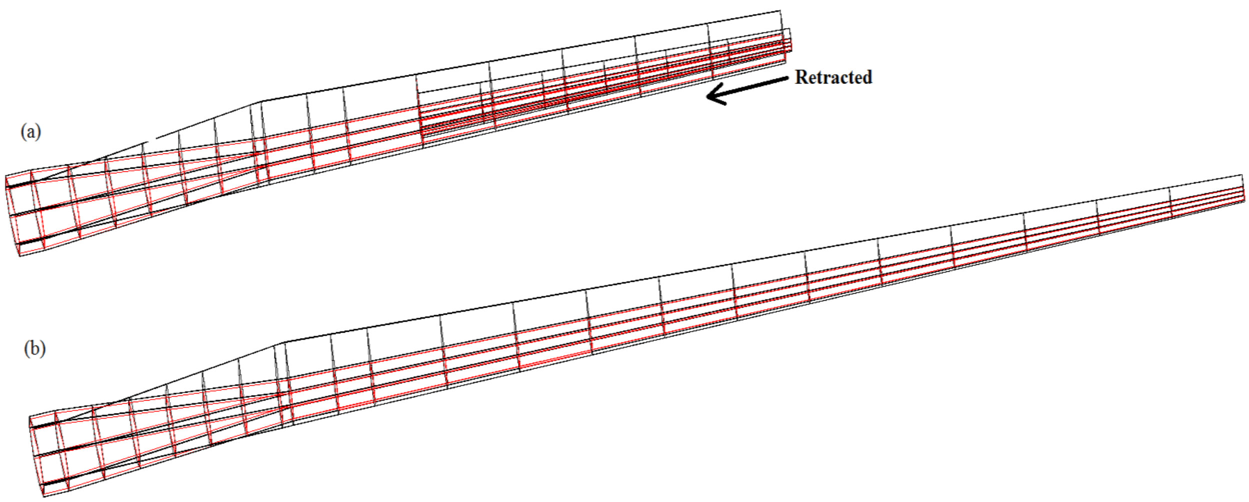

Figure 1.1: A 3-Dimensional representation of (a).extendable wind turbine blade and (b).conventional wind turbine blade.

The parameters computed in this study include the static deflection, stresses, and natural frequency of vibration of the extendable wind turbine blade in its retracted positions in comparison to the fully extended conventional wind turbine blade. Initially a basic model was developed for the wind turbine blade adopting the S818 [2] airfoil shape for the conventional blade. The same shape/geometry was used to generate a three-dimensional finite element model of the turbine blade using AutoCAD 2014.

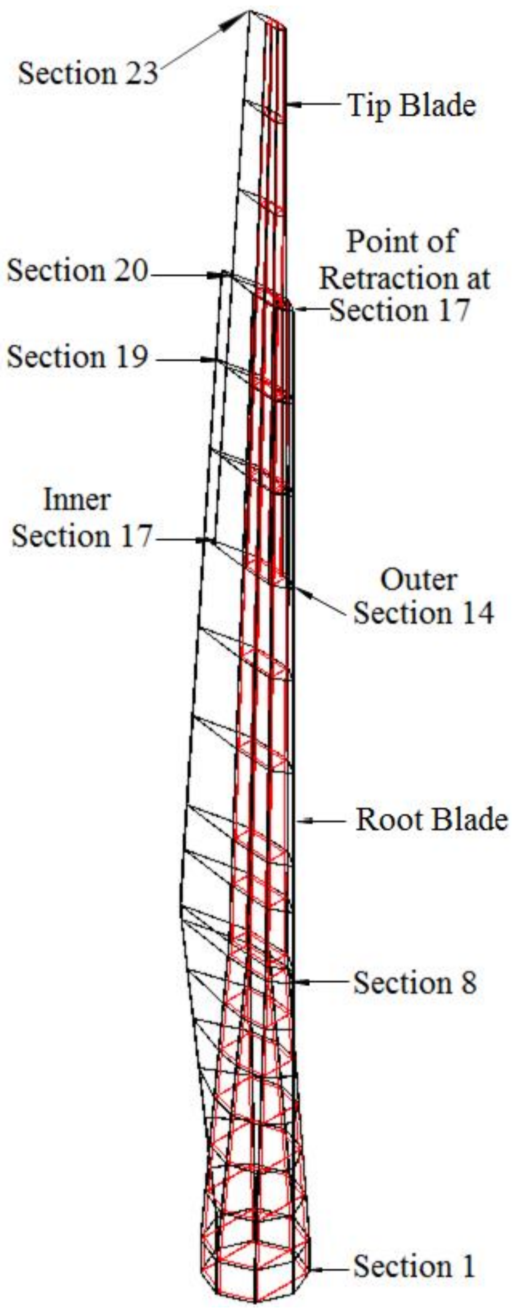

Figure 1.2: Diagrammatic Representation of Partly Retracted Blade 7

After the modelling phase all the geometry, material and loading details were used for computing the results using FORTRAN. For the calculation of static deflections and stresses, the analysis was completed for two load cases.

The Load cases are:

1. **Wind Load only**
2. **Dead Load+ Wind Load**

Load case 1 specifically gives an idea of the amount of deflection occurring solely due to the incident wind load and the 2nd load case gives results that are more practical to compare. For both the load cases, comparisons were made between the conventional blade and the various retracted blades. The calculated results include comparison of:

1. Static Deflection
2. Longitudinal And Transverse Stresses
3. Fundamental frequency of Vibration, And
4. Modes of Vibration of the Blades.

Results also include:

1. Net Shear Force acting at the end of the Root Blade (Figure 1.2), And
2. Bending moment at the root of the various Retractable Blades.

CHAPTER 2: LITERATURE REVIEW

Wind turbines have been used from ancient times beginning with windmills dating back to about 2000 B.C. in ancient Babylon [3]. A significant development occurred in 1887 [4], when the first electricity-generating wind turbine was devised by a Scottish academic, James Blyth. The first megawatt-class wind turbine (1.25MW), known as the Smith-Putnam wind turbine was developed in the fall of 1941[4] [5]. During their development the higher performance and power production required an increase in the size of the turbine. It had 75-foot long two-blades. In 1956 Johannes Juul [4] [6] developed the first 3-bladed wind turbine known as the Gedser Wind Turbine, which would influence many of the commercial wind turbine blade designs in the time followed.

From this point the size of turbines began to get even larger because of the higher power they generated. To make the power generated even more effective, wind farms were developed. The first known wind farm was started in 1980 [4] at New Hampshire and consisted 20- 30kW turbines. Presently there are a number of wind farms and numerous wind farms are expected to be installed in onshore and offshore sites in the coming decades [7]. An issue that concerns setting up multiple wind turbines in a farm is the interaction of individual turbines with the other turbines in the wind farm. Specifically, according to Sørensen et al. [8] turbulence intensity drastically increases in the wakes behind each turbine while at the same time the mean wind speed decreases. Hence the already complex problem of understanding the behavior of single wind turbine to the incident wind becomes even more complicated when considering the variance in mean flow and local turbulence. Yet understanding these interactions are an integral part to make decisions regarding the optimal placement and spacing of turbines within a geometric space so that power generation is optimized while simultaneously ensuring that the mechanical and structural stability of the turbine structural system is not compromised. At the same time, issues related to large deformation behavior in turbine blade response have grown as the length of the blades has increased.

Wind turbines have also been growing in size over the last few decades. Turbines with a nominal power of 10MW rotor diameter nearing several hundred meters are under both theoretical and practical considerations. The largest wind turbine in use is ENERCON'S E126 7.5MW [9] with a rotor diameter is 126 m. The blades of the turbine usually account for about 15% of the total turbine cost and are usually designed for covering maximum of the swept area (the circular area swept by the turning blades). Hence to ensure larger swept area, blades had to be longer, allowing its higher placement on towers and thereby capturing higher wind speeds. Power generated from wind is proportional to the cube of wind speed, yielding another reason to increase blade length [10]. Yet most blade designs are currently based on a variation of a rotating cantilever beam. In such a case, the linearized stiffness for a blade under the commonly used assumption of Euler-Bernoulli beam theory is linearly related to the product of extensional modulus multiplied by the second moment of the area, but inversely proportional to the cube of the beam length. Hence as the beam grows in length, there is a much stronger tendency for the beam behavior to include nonlinear effects. Additionally, increases in blade length can lead to undesirable vibration characteristics related to unwanted resonances and the coupling of bending and torsional modes that can lead to aeroelastic instability (Riziotis et al. [11]). These concerns multiply as the blade lengthens.

Similar considerations exist for turbulent wind flows (Moriarty et al. [12]). The size and spacing of the wind turbines within a wind farm are crucial design parameters that can influence the level of wind loading on the turbines along a representative column of land. The level of relative disruption of uniform flow even past fixed objects is still a subject of intense study, and coupling the interactions of the velocity fields with rotating and flexible turbine blades has seen very little investigation. Yet these interactions are crucial for a performance-based assessment of turbines that can include both optimal operating conditions and a reasonable control of the level of stresses that may lead to fatigue damage or localized failures during periods of high wind.

There is an additional set of concerns that has received increased attention as turbine blades have increased in length, and that is the difficulty of transporting the blades using available roads, highways, and rail lines. Specifically: 1) several countries have limits on the lengths of objects that can be transported [13], and special permits for exceptions add to time considerations and are not automatic, 2) because of the specialized nature of turbine construction equipment, any delays related to transportation can cause a disproportionate increase in cost, 3) many observers have echoed the report of Swedish business reporter Erik Palm: “Problems with transportation could limit the size of new land-based turbines. Going around road corners and narrow bridges with 50-yard blades is already a problem, and the only thing that could alleviate that would be technology for making multiple-piece blades.” Figure 2.1, 2.2 and 2.3 shows recent photos highlighting these issues.

Figure 2.1**:** An accident in Dubuque, Iowa in January 2013 caused $277,000 in damage to the rigs and 160-foot blades and stalled traffic for several hours (Telegraph Herald).

Figure 2.2: A 30 ton blade transported on road across Funen and Jutland in Denmark, July 2013 (Danish Television).

Figure 2.3: A 75 meter Siemens blade being driven over a roundabout berm in Denmark in August 2012.

One possible design that could provide some benefit in some circumstance is the extendable blades for the turbines. These are also referred to as retractable turbine blades, variable length turbine blades, or telescopic blades. There are very few studies that have been conducted for these designs. The earliest known development of the extendable wind turbine was mentioned in a Study conducted by Pasupuleti [1] about the development of a variable length wind turbine blade by Energy Unlimited Inc. They retrofitted an existing wind turbine (120 KW Bonus wind turbine) with a proof of concept prototype. The turbine blades (initially 7.5 m) were made to be extendable up to 12 m. The variblade used in Pasupuleti's study is as shown below in Figure 2.4.

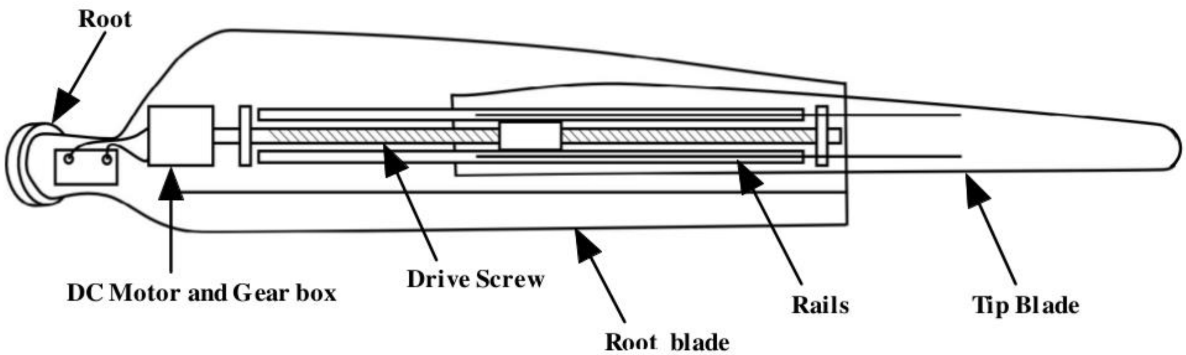

Figure 2.4: Variblade and its components from [1]

According to his study with the increase in rotor size mechanical stability reduces. Hence the rotor has to be small when the wind load is high to maintain the stability of the turbine. To harvest more power during low wind loading, the rotor size can be increased. If the blades can be designed to retract during high wind load conditions it can increase mechanical stability, and could extend to the full length during low wind loading to capture more wind for power. Such a model of use could help to optimize blade performance. This was the principle behind the function of the above mentioned variblade. In addition to this in Pasupuleti's study, he was also able to conclude that with an increase in blade length of 20%, the performance of the blade would be improved by 44% and the net energy output would be improved by about 33%.This study was strictly to measure the power generated by the variblade properties such as fundamental frequency and stress generated in the extendable blade due to applied load was not computed.

This type of blade was further analyzed and tested in depth by Sharma [14] where the performance of the turbine at given conditions was investigated using a mathematical model based on blade element-momentum theory. He considered wind speed data of Auckland, NZ. The model also incorporated a Weibull wind speed distribution to enable the calculation of annual energy output as criteria of comparison. The study also had a first order cost analysis between the extendable blade and the standard blade. The study concluded that the wind turbines, whose diameter could be doubled, produced twice as much power as that corresponding to a turbine with fixed length blades. The study also conducted cost analysis which gave positive results. Imaan, Sharma and Flay [15] [16] conducted a study in a specific region in New Zealand and found that there was an 18% increase in annual energy production of a 10kW wind turbine with telescopic blades.

Tartibu et al. [17] conducted modal analysis on blades similar to that of the wind turbine blades aiming to study the relative modal shift when the blades were fully extended compared to the frequencies when the blades were fully extended. This paper considered a very simple model for the blade without detailed geometrical shape and details, essentially considering it as a simple beam with constant cross-section. The analysis was performed treating the beam as a one-dimensional Euler-Bernoulli Beam element. Improving on this type of simple model is one of the aims of the present study. Additional studies by McCoy and Griffin [18] [19] focused mainly on aerodynamic and control aspects of this class of turbine blade. This study included simulations using MSC-ADAMS and detailed cost modelling based on the simulated loads.

Two of the key characteristics of blade design are the blade bending modes and fatigue cycling. Both are highly dependent on the structural response to both static and transient loading. The fundamental blade frequency typically causes the largest deflections in the blade that induce a smooth curve over the entire domain of the blade length. If this frequency is close to the rotor’s rotational frequency, the induced vibrational response of the blades to simple rotational motion can cause large amplitude resonance even without any wind loading. For this reason, most blades are designed so that the fundamental bending frequency is well above that of the angular frequency of the rotor. For larger blades, these frequencies and resulting mode shapes can be amplitude dependent – a condition rarely investigated in most blade designs. Additionally, as the blades rotate they are subjected to induced gravitational loads that reverse sign on either side of the rotational path, cycling stress sign at a fairly high rate. Most blades are nominally designed for a 20-year lifespan, allowing for about 5 million cycles over the course of expected use. Once again, large blades with both shear-deformable and large deformation behaviors can dramatically influence the level of stress within the blade.

There has been significant number of studies on nonlinear and/or large-deformation studies of turbine blades, ranging in chronology from the historical development of Hodges and Dowell [20] for general rotor blades up to the recent work of Larsen and Nielsen [21] and references therein. All of these models have demonstrated the likelihood of significant changes in design stresses when beams become more flexible. Even more important, the increased use of composites, which can include typical fiberglass elements but are beginning to move towards carbon-fiber reinforced components, can yield levels of shear deformation that will dramatically change analysis and behavior of turbine blades. In this study the effects of shear deformation are included by modeling the blade as an anisotropic solid.

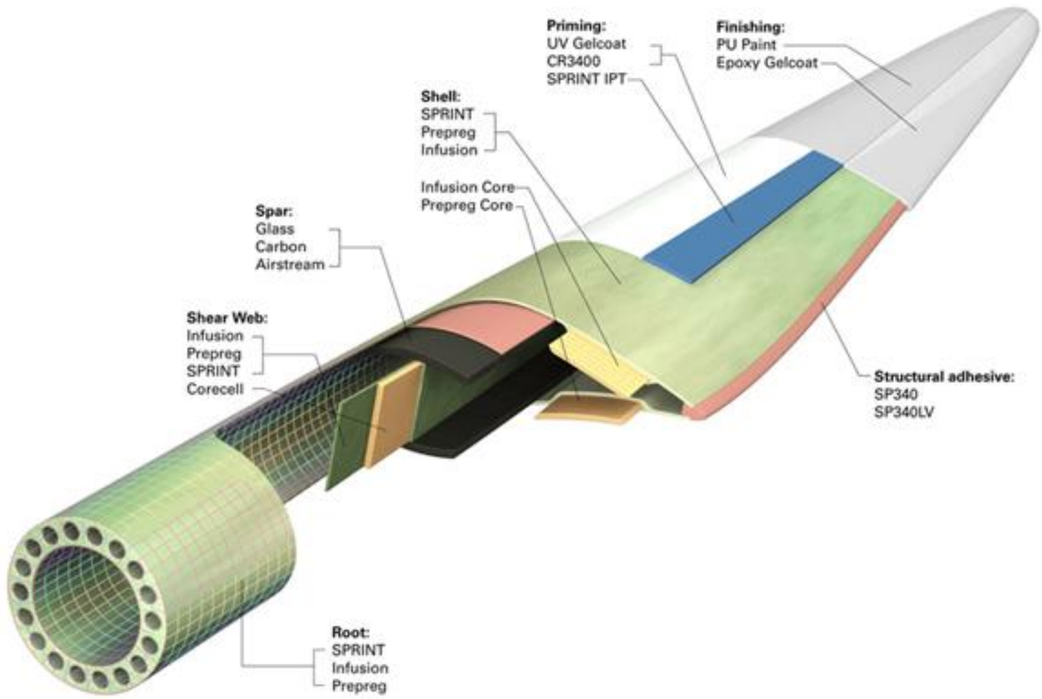

Figure 2.5: Cross-sectional details of a wind turbine blade [22].

Rotor blade components usually take advantage of box spar designs, in which the blade skins are often manufactured separately and then bonded together along with the structural box spar in between. In Figure 2.5 the detailed configuration of the skin and box spar are shown. The spar (spar cap) and the shear web together constitute the box spar. This assembly contributes the most weight for the entire blade and is responsible for the structural stability and effectiveness of the entire blade. More detailed diagrams are included in later chapters. A large number of material components have been used, or are proposed for use, for these structural elements. In this research we consider standard blade cross-sections that will be modeled with continuum theories of deformation, specifically the three-dimensional equations of elasticity.

CHAPTER 3: THEORY

In this chapter the governing equations are presented and the how they are used to solve our static problem. This chapter also provides details about how the blade was modelled, assumptions that were made, details of the blade model including geometry of the blade and the material properties and various retracted blades that were included for analysis. Section 3.1 below explains how nodal displacement and fundamental frequency can be derived from the governing equations.

3.1: Weak Form

3.1.1: Equations of Motion

Equilibrium Equations of Motion in 3-D are:

$$\frac{\partial \sigma_{xx}}{\partial x} + \frac{\partial \sigma_{xy}}{\partial y} + \frac{\partial \sigma_{xz}}{\partial z} + f_x = \rho\ \frac{\partial^2 u}{\partial t^2}$$

$$\frac{\partial \sigma_{yx}}{\partial x} + \frac{\partial \sigma_{yy}}{\partial y} + \frac{\partial \sigma_{yz}}{\partial z} + f_y = \rho\ \frac{\partial^2 v}{\partial t^2} \tag{3.1}$$

$$\frac{\partial \sigma_{zx}}{\partial x} + \frac{\partial \sigma_{zy}}{\partial y} + \frac{\partial \sigma_{zz}}{\partial z} + f_z = \rho\ \frac{\partial^2 w}{\partial t^2},$$

In the V, volume domain

Here u(x, y, z, t), v(x, y, z, t) and w(x, y, z, t) are the displacements in the x, y and z directions.

Strain Displacements are:

$$\varepsilon_x = \frac{\partial u}{\partial x}$$

$$\varepsilon_y = \frac{\partial v}{\partial y}$$

$$\varepsilon_z = \frac{\partial w}{\partial z}$$

$$\gamma_{xy} = \frac{\partial u}{\partial y} + \frac{\partial v}{\partial x}$$

$$\gamma_{yz} = \frac{\partial v}{\partial z} + \frac{\partial w}{\partial y}$$

$$\gamma_{zx} = \frac{\partial w}{\partial x} + \frac{\partial u}{\partial z}$$

And, The Stress-Strain Relations are:

$$\sigma_{xx} = \sigma_x = C_{11}\varepsilon_x + C_{12}\varepsilon_y + C_{13}\varepsilon_z \tag{3.2}$$

$$\sigma_{yy} = \sigma_y = C_{12}\varepsilon_x + C_{22}\varepsilon_y + C_{23}\varepsilon_z$$

$$\sigma_{zz} = \sigma_z = C_{13}\varepsilon_x + C_{23}\varepsilon_y + C_{33}\varepsilon_z$$

$$\sigma_{xy} = \tau_{xy} = C_{66}\gamma_{xy}\,, \qquad \sigma_{yz} = \tau_{yz} = C_{44}\gamma_{yz}$$

$$\sigma_{xz} = \tau_{xz} = C_{55}\gamma_{xz}$$

The Compliance matrix shown below is used to compute the stiffness matrix,

$$[S]=\begin{bmatrix} S_{11} & S_{12} & S_{13} & 0 & 0 & 0 \\ S_{12} & S_{22} & S_{23} & 0 & 0 & 0 \\ S_{13} & S_{23} & S_{33} & 0 & 0 & 0 \\ 0 & 0 & 0 & S_{44} & 0 & 0 \\ 0 & 0 & 0 & 0 & S_{55} & 0 \\ 0 & 0 & 0 & 0 & 0 & S_{66} \end{bmatrix} = \begin{bmatrix} \frac{1}{E_1} & \frac{-v_{12}}{E_2} & \frac{-v_{13}}{E_3} & 0 & 0 & 0 \\ \frac{-v_{12}}{E_1} & \frac{1}{E_2} & \frac{-v_{23}}{E_3} & 0 & 0 & 0 \\ \frac{-v_{13}}{E_1} & \frac{-v_{23}}{E_2} & \frac{1}{E_3} & 0 & 0 & 0 \\ 0 & 0 & 0 & \frac{1}{G_{23}} & 0 & 0 \\ 0 & 0 & 0 & 0 & \frac{1}{G_{13}} & 0 \\ 0 & 0 & 0 & 0 & 0 & \frac{1}{G_{12}} \end{bmatrix}$$

Hence we get the Stiffness matrix by inverting the compliance matrix.

$$C_{11} = \frac{S_{33}S_{22} - {S_{23}}^2}{S}, \qquad C_{22} = \frac{S_{33}S_{11} - {S_{13}}^2}{S}$$

$$C_{33} = \frac{S_{11}S_{22} - {S_{12}}^2}{S}, \qquad C_{12} = \frac{-(S_{12}S_{33} - S_{13}S_{23})}{S}$$

$$C_{13} = \frac{-(S_{13}S_{22} - S_{12}S_{23})}{S}, \qquad C_{23} = \frac{-(S_{23}S_{11} - S_{12}S_{13})}{S}$$

$$C_{44} = \frac{1}{S_{44}}, \qquad C_{55} = \frac{1}{S_{55}}, \qquad C_{66} = \frac{1}{S_{66}}$$

Here,

$$S = S_{11}S_{22}S_{33} - S_{11}S_{23}S_{23} - S_{22}S_{13}S_{13} - S_{33}S_{12}S_{12} + 2S_{12}S_{23}S_{13}$$

3.1.2: Final Form of Equilibrium Equations

$$\frac{\partial}{\partial x}\left(C_{11}\frac{\partial u}{\partial x}+C_{12}\frac{\partial v}{\partial y}+C_{13}\frac{\partial w}{\partial z}\right)+C_{66}\frac{\partial}{\partial y}\left(\frac{\partial u}{\partial y}+\frac{\partial v}{\partial x}\right)+C_{55}\frac{\partial}{\partial z}\left(\frac{\partial w}{\partial x}+\frac{\partial u}{\partial z}\right)+f_x=\rho\ \frac{\partial^2 u}{\partial t^2}$$

$$C_{66}\frac{\partial}{\partial x}\left(\frac{\partial u}{\partial y}+\frac{\partial v}{\partial x}\right)+\frac{\partial}{\partial y}\left(C_{21}\frac{\partial u}{\partial x}+C_{22}\frac{\partial v}{\partial y}+C_{23}\frac{\partial w}{\partial z}\right)+C_{44}\frac{\partial}{\partial z}\left(\frac{\partial v}{\partial z}+\frac{\partial w}{\partial y}\right)+f_y=\rho\ \frac{\partial^2 v}{\partial t^2}$$

$$C_{55}\frac{\partial}{\partial x}\left(\frac{\partial w}{\partial x}+\frac{\partial u}{\partial z}\right)+C_{44}\frac{\partial}{\partial y}\left(\frac{\partial v}{\partial z}+\frac{\partial w}{\partial y}\right)+\frac{\partial}{\partial z}\left(C_{31}\frac{\partial u}{\partial x}+C_{32}\frac{\partial v}{\partial y}+C_{33}\frac{\partial w}{\partial z}\right)+f_z=\rho\ \frac{\partial^2 w}{\partial t^2},$$

In the V, volume domain

3.1.3: Weak form equations for Finite Element Analysis

So applying this in Finite Element Analysis, we discretize the stress and strain limiting it to each element and then integrate it over the whole domain, V.

Hence the Equilibrium Equations for Finite Element Analysis (Weak Form Equations) are:

$$\int_V v_1\left(\frac{\partial}{\partial x}\left(C_{11}\frac{\partial u}{\partial x}+C_{12}\frac{\partial v}{\partial y}+C_{13}\frac{\partial w}{\partial z}\right)+C_{66}\frac{\partial}{\partial y}\left(\frac{\partial u}{\partial y}+\frac{\partial v}{\partial x}\right)+C_{55}\frac{\partial}{\partial z}\left(\frac{\partial w}{\partial x}+\frac{\partial u}{\partial z}\right)+f_x\right.$$
$$\left.-\left(\rho\ \frac{\partial^2 u}{\partial t^2}\right)\right)dxdydz=0$$

$$\int_V v_2 \left(C_{66} \frac{\partial}{\partial x}\left(\frac{\partial u}{\partial y} + \frac{\partial v}{\partial x}\right) + \frac{\partial}{\partial y}\left(C_{21}\frac{\partial u}{\partial x} + C_{22}\frac{\partial v}{\partial y} + C_{23}\frac{\partial w}{\partial z}\right) + C_{44}\frac{\partial}{\partial z}\left(\frac{\partial v}{\partial z} + \frac{\partial w}{\partial y}\right) + f_y - \left(\rho\, \frac{\partial^2 v}{\partial t^2}\right)\right) dxdydz = 0$$

$$\int_V v_3 \left(C_{55} \frac{\partial}{\partial x}\left(\frac{\partial w}{\partial x} + \frac{\partial u}{\partial z}\right) + C_{44}\frac{\partial}{\partial y}\left(\frac{\partial v}{\partial z} + \frac{\partial w}{\partial y}\right) + \frac{\partial}{\partial z}\left(C_{31}\frac{\partial u}{\partial x} + C_{32}\frac{\partial v}{\partial y} + C_{33}\frac{\partial w}{\partial z}\right) + f_z - \left(\rho\, \frac{\partial^2 w}{\partial t^2}\right)\right) dxdydz = 0$$

They are further condensed to,

$$\int_V \left(C_{11}\frac{\partial v_1}{\partial x}\frac{\partial u}{\partial x} + C_{12}\frac{\partial v_1}{\partial x}\frac{\partial v}{\partial y} + C_{13}\frac{\partial v_1}{\partial x}\frac{\partial w}{\partial z} + C_{66}\frac{\partial v_1}{\partial y}\frac{\partial u}{\partial y} + C_{66}\frac{\partial v_1}{\partial y}\frac{\partial v}{\partial x} + C_{55}\frac{\partial v_1}{\partial z}\frac{\partial w}{\partial x} + C_{55}\frac{\partial v_1}{\partial z}\frac{\partial u}{\partial z} + f_x v_1 - \left(\rho\, \frac{\partial^2 u}{\partial t^2}\right) v_1 \right) dxdydz - \oint_r v_1(t_x)\, ds = 0$$

$$\int_V \left(C_{66}\frac{\partial v_2}{\partial x}\frac{\partial u}{\partial y} + C_{66}\frac{\partial v_2}{\partial x}\frac{\partial v}{\partial x} + C_{21}\frac{\partial v_2}{\partial y}\frac{\partial u}{\partial x} + C_{22}\frac{\partial v_2}{\partial y}\frac{\partial v}{\partial y} + C_{23}\frac{\partial v_2}{\partial y}\frac{\partial w}{\partial z} + C_{44}\frac{\partial v_2}{\partial z}\frac{\partial v}{\partial z} + C_{44}\frac{\partial v_2}{\partial z}\frac{\partial w}{\partial y} + f_y v_2 - \left(\rho\, \frac{\partial^2 v}{\partial t^2}\right) v_2 \right) dxdydz - \oint_r v_2(t_y)\, ds = 0 \qquad (3.3)$$

$$\int_V \left(C_{55}\frac{\partial v_3}{\partial x}\frac{\partial w}{\partial x} + C_{55}\frac{\partial v_3}{\partial x}\frac{\partial u}{\partial z} + C_{44}\frac{\partial v_3}{\partial y}\frac{\partial v}{\partial z} + C_{44}\frac{\partial v_3}{\partial y}\frac{\partial w}{\partial y} + C_{31}\frac{\partial v_3}{\partial z}\frac{\partial u}{\partial x} + C_{32}\frac{\partial v_3}{\partial z}\frac{\partial v}{\partial y} \right.$$

$$\left. + C_{33}\frac{\partial v_3}{\partial z}\frac{\partial w}{\partial z} + f_y v_3 - \left(\rho\ \frac{\partial^2 w}{\partial t^2}\right) v_3 \right) dxdydz - \oint_r v_3(t_z)ds = 0$$

Here,

$$t_x = \left(C_{11}\frac{\partial u}{\partial x} + C_{12}\frac{\partial v}{\partial y} + C_{13}\frac{\partial w}{\partial z}\right) n_x + \left(C_{66}\frac{\partial u}{\partial y} + C_{66}\frac{\partial v}{\partial x}\right) n_y + \left(C_{55}\frac{\partial w}{\partial x} + C_{55}\frac{\partial u}{\partial z}\right) n_z$$

$$t_y = \left(C_{66}\frac{\partial u}{\partial y} + C_{66}\frac{\partial v}{\partial x}\right) n_x + \left(C_{21}\frac{\partial u}{\partial x} + C_{22}\frac{\partial v}{\partial y} + C_{23}\frac{\partial w}{\partial z}\right) n_y + \left(C_{44}\frac{\partial v}{\partial z} + C_{44}\frac{\partial w}{\partial y}\right) n_z$$

$$t_z = \left(C_{55}\frac{\partial w}{\partial x} + C_{55}\frac{\partial u}{\partial z}\right) n_x + \left(C_{44}\frac{\partial v}{\partial z} + C_{44}\frac{\partial w}{\partial y}\right) n_y + \left(C_{31}\frac{\partial u}{\partial x} + C_{32}\frac{\partial v}{\partial y} + C_{33}\frac{\partial w}{\partial z}\right) n_z$$

Boundary conditions are specified in two ways:-

1. EBCs(Elastic Boundary Conditions): Specifies u, v or w
2. NBCs(Natural Boundary Conditions): Specifies t_x , t_y or t_z

For specific cases we would know u or t_x, v or t_y and w or t_z at every boundary.

3.1.4: Weak Form Equations with Approximation

Here we initially approximate u, v and w as,

$$u(x, y, z, t) = u(x, y, z) \sin \omega t$$

$$v(x, y, z, t) = v(x, y, z) \sin \omega t$$

$$w(x, y, z, t) = w(x, y, z) \sin \omega t$$

For Finite Element Approximation, we approximate u(x, y, z), v(x, y, z), w(x, y, z), v_1, v_2, v_3 as below.

$$u = \sum_{j=1}^{n} u_j \psi_j^u, \qquad v = \sum_{j=1}^{n} v_j \psi_j^v, \qquad w = \sum_{j=1}^{n} w_j \psi_j^w$$

$$v_1 = \psi_i^u, \qquad v_2 = \psi_i^v, \qquad v_3 = \psi_i^w$$

Keeping the approximation functions same allows us to maintain element symmetry.

And substituting this into the weak form gives,

$$K_{ij}^{11} u_i + K_{ij}^{12} v_i + K_{ij}^{13} w_i = F_i^1 - \omega^2 M_{ij}^{11} u_i$$

$$K_{ij}^{21} u_i + K_{ij}^{22} v_i + K_{ij}^{23} w_i = F_i^2 - \omega^2 M_{ij}^{22} v_i$$

$$K_{ij}^{31} u_i + K_{ij}^{32} v_i + K_{ij}^{33} w_i = F_i^3 - \omega^2 M_{ij}^{33} w_i$$

Or in matrix form,

$$\begin{bmatrix} [K^{11}] & [K^{12}] & [K^{13}] \\ [K^{21}] & [K^{22}] & [K^{23}] \\ [K^{31}] & [K^{32}] & [K^{33}] \end{bmatrix} \begin{Bmatrix} \{u\} \\ \{v\} \\ \{w\} \end{Bmatrix} = \begin{Bmatrix} \{F^1\} \\ \{F^2\} \\ \{F^3\} \end{Bmatrix} - \omega^2 \begin{bmatrix} [M^{11}] & [0] & [0] \\ [0] & [M^{22}] & [0] \\ [0] & [0] & [M^{33}] \end{bmatrix} \begin{Bmatrix} \{u\} \\ \{v\} \\ \{w\} \end{Bmatrix}, \quad (3.4)$$

Where,

1. $\begin{bmatrix} [K^{11}] & [K^{12}] & [K^{13}] \\ [K^{21}] & [K^{22}] & [K^{23}] \\ [K^{31}] & [K^{32}] & [K^{33}] \end{bmatrix}$ Is the stiffness matrix.

And the corresponding elements of the matrix are,

$$K_{ij}^{11} = \int_V \left(C_{11} \frac{\partial \psi_i^u}{\partial x} \frac{\partial \psi_j^u}{\partial x} + C_{66} \frac{\partial \psi_i^u}{\partial y} \frac{\partial \psi_j^u}{\partial y} + C_{55} \frac{\partial \psi_i^u}{\partial z} \frac{\partial \psi_j^u}{\partial z} \right) dxdydz$$

$$K_{ij}^{12} = \int_V \left(C_{12} \frac{\partial \psi_i^u}{\partial x} \frac{\partial \psi_j^w}{\partial y} + C_{66} \frac{\partial \psi_i^u}{\partial y} \frac{\partial \psi_j^w}{\partial x} \right) dxdydz$$

$$K_{ij}^{13} = \int_V \left(C_{13} \frac{\partial \psi_i^u}{\partial x} \frac{\partial \psi_j^w}{\partial z} + C_{55} \frac{\partial \psi_i^u}{\partial z} \frac{\partial \psi_j^w}{\partial x} \right) dxdydz$$

$$K_{ij}^{21} = \int_V \left(C_{66} \frac{\partial \psi_i^v}{\partial x} \frac{\partial \psi_j^u}{\partial y} + C_{21} \frac{\partial \psi_i^v}{\partial y} \frac{\partial \psi_j^u}{\partial x} \right) dxdydz$$

$$K_{ij}^{22} = \int_V \left(C_{66} \frac{\partial \psi_i^v}{\partial x} \frac{\partial \psi_j^v}{\partial x} + C_{22} \frac{\partial \psi_i^v}{\partial y} \frac{\partial \psi_j^v}{\partial y} + C_{44} \frac{\partial \psi_i^v}{\partial z} \frac{\partial \psi_j^v}{\partial z} \right) dxdydz$$

$$K_{ij}^{23} = \int_V \left(C_{23} \frac{\partial \psi_i^v}{\partial y} \frac{\partial \psi_j^w}{\partial z} + C_{44} \frac{\partial \psi_i^v}{\partial z} \frac{\partial \psi_j^w}{\partial y} \right) dxdydz$$

$$K_{ij}^{31} = \int_V \left(C_{55} \frac{\partial \psi_i^w}{\partial x} \frac{\partial \psi_j^u}{\partial z} + C_{31} \frac{\partial \psi_i^w}{\partial z} \frac{\partial \psi_j^u}{\partial x} \right) dxdydz$$

$$K_{ij}^{32} = \int_V \left(C_{44} \frac{\partial \psi_i^w}{\partial y} \frac{\partial \psi_j^v}{\partial z} + C_{32} \frac{\partial \psi_i^w}{\partial z} \frac{\partial \psi_j^v}{\partial y} \right) dxdydz$$

$$K_{ij}^{33} = \int_V \left(C_{55} \frac{\partial \psi_i^w}{\partial x} \frac{\partial \psi_j^w}{\partial x} + C_{44} \frac{\partial \psi_i^w}{\partial y} \frac{\partial \psi_j^w}{\partial y} + C_{33} \frac{\partial \psi_i^w}{\partial z} \frac{\partial \psi_j^w}{\partial z} \right) dxdydz$$

2. $\begin{bmatrix} [M^{11}] & [0] & [0] \\ [0] & [M^{22}] & [0] \\ [0] & [0] & [M^{33}] \end{bmatrix}$ is the mass matrix.

And the corresponding elements of the matrix are,

$$M_{ij}^{11} = \int_V \rho \, \psi_i^u \psi_j^u dxdydz$$

$$M_{ij}^{22} = \int_V \rho \, \psi_i^v \psi_j^v dxdydz$$

$$M_{ij}^{33} = \int_V \rho \, \psi_i^w \psi_j^w dxdydz$$

3. $\begin{Bmatrix} \{F^1\} \\ \{F^2\} \\ \{F^3\} \end{Bmatrix}$ is the Force Fector.

Its corresponding elements are,

$$F_i^1 = \int_V f_x \psi_i^u dxdydz + \oint_r t_x \psi_i^u ds$$

$$F_i^2 = \int_V f_y \psi_i^v dxdydz + \oint_r t_y \psi_i^v ds$$

$$F_i^1 = \int_V f_z \psi_i^w dxdydz + \oint_r t_z \psi_i^w ds$$

3.2: Weak Form Equation for Calculating Static Deflection and Stresses

Since the analysis for static deflection is time independent, ω=0. Hence we have weak form equation for calculating static deflection as,

$$\begin{bmatrix} [K^{11}] & [K^{12}] & [K^{13}] \\ [K^{21}] & [K^{22}] & [K^{23}] \\ [K^{31}] & [K^{32}] & [K^{33}] \end{bmatrix} \begin{Bmatrix} \{u\} \\ \{v\} \\ \{w\} \end{Bmatrix} = \begin{Bmatrix} \{F^1\} \\ \{F^2\} \\ \{F^3\} \end{Bmatrix} \tag{3.5}$$

3.3: Weak Form Equation for Vibration Analysis

Since the analysis for fundamental frequency of vibration does not involve external loading, Force vector = 0. Hence we have the weak form equation for computing free vibration as,

$$\begin{bmatrix} [K^{11}] & [K^{12}] & [K^{13}] \\ [K^{21}] & [K^{22}] & [K^{23}] \\ [K^{31}] & [K^{32}] & [K^{33}] \end{bmatrix} \begin{Bmatrix} \{u\} \\ \{v\} \\ \{w\} \end{Bmatrix} = -\omega^2 \begin{bmatrix} [M^{11}] & [0] & [0] \\ [0] & [M^{22}] & [0] \\ [0] & [0] & [M^{33}] \end{bmatrix} \begin{Bmatrix} \{u\} \\ \{v\} \\ \{w\} \end{Bmatrix} \tag{3.6}$$

Here the equation is of the format,

$$[A]\{X\} = \lambda[B]\{X\}$$

This can be solved by treating it as a Generalized Eigen Value Problem.

3.4: Minimizing Bandwidth

To minimize the bandwidth, we need to store the assembled system using the following.

We have,

$$\begin{bmatrix} u_1 \\ u_2 \\ u_3 \\ u_4 \\ \vdots \\ v_{n-1} \\ v_n \end{bmatrix}$$

But what we want is,

$$\begin{bmatrix} u_1 \\ v_1 \\ u_2 \\ v_2 \\ \vdots \\ u_n \\ v_n \end{bmatrix}$$

This is a straight forward step that can be managed as long as we keep the indexing correct.

3.5: Material and Geometric Details of the Blade

A basic model of the blade was developed using AutoCAD 2014 and was modeled using the blade outlined in a study conducted at the Sandia National Laboratory by Griffin [2]. Before explaining the details of the blade model, a few assumptions considered for effective modelling. The assumptions are:

1. A course mesh is modelled for the blade so the root is not circular and the other sections don't have a regular airfoil shape.
2. Shell is assume to be made of glass fiber composite and typical glass fiber properties were used instead of considering a laminate stack up of balsa, tri-axial fibers, gel coat, etc.
3. For analysis of retractable turbine blades, instead of treating the blade to have two parts (root blade and tip blade), the mass of the tip blade was added to that of root blade, and treated as a single unit. Further, details of this assumption are explained in section 3.7 of Chapter 3.
4. Wind pressure is assumed to be the same throughout the blade, though in a practical scenario it varies throughout the length of the blade depending on elevation and the orientation of the blade.
5. Typical material properties were assumed for the shell and the box spar.
6. Thickness of the materials was assumed to vary depending on how big or small the cross-sectional area was.

7. The retracted blades, namely Blades 2 to 7 are not retracted positions of the same blade, but different retracted blades having different root blade and tip blade lengths. But all the blades have same extended blade lengths.

Sandia's blade model [2] has a length of 100 m with an S818 airfoil shape (Figure 3.2). The same airfoil shape has been used in this paper for analysis. The blade has a solid frame of a box spar which accounts for most of the blade enabling necessary strength and rigidity to the blade. There is a thin layer of skin enclosing the box spar. Each of these materials has varying material properties (Figure 3.2).

The blade's longitudinal profile along the long axis of the blade is depicted in figure 3.1. In the figure R is the radius of the turbine, R=35 m. The parameters in the graph are expressed relative to this dimension. The root of the blade starts at r/R=0.05 and remains circular till r/R=0.07.It then transitions to an airfoil shape until r/R=0.25, where it has the S818 airfoil profile. The blade therefore has the airfoil shape from r/R=0.25 to r/R=1, which is 26.25m. The S818 airfoil shape is as shown in figure 3.2. Its dimensions are relative to its maximum chord length and it varies depending on the section considered.

From the above data we have a 33.25 m (35 m from the center of the rotor) long blade. It is circular for 0.7 m from the root and a diameter of 2 m. It transitions from the circular shape to the airfoil shape for 6.3 m. The blade has a maximum chord length of 2.84 m at this point and then it tapers for the rest of the length with the airfoil shape to 0.91 m chord length. The blade was modelled specifically to compute and compare the static deflection and fundamental frequency of conventional blade and extendable blade and not modelled for detailed blade design. Hence the model approximates details such as the number of layers of polymer used, adhesive layer thickness between the skin and the box spar and possible inaccuracy due to simplified model for analysis. The main interest is the change in bulk response for a blade that is extended versus one that is fully extended.

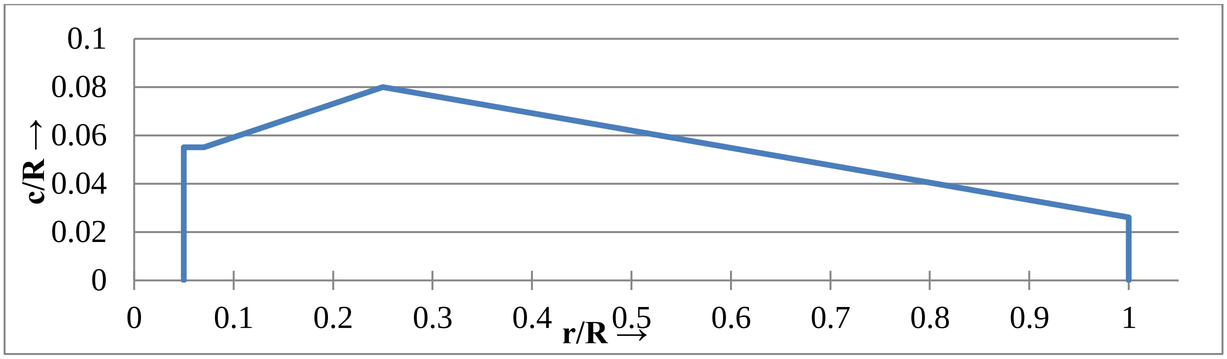

Figure 3.1: Longitudinal profile of the model blade

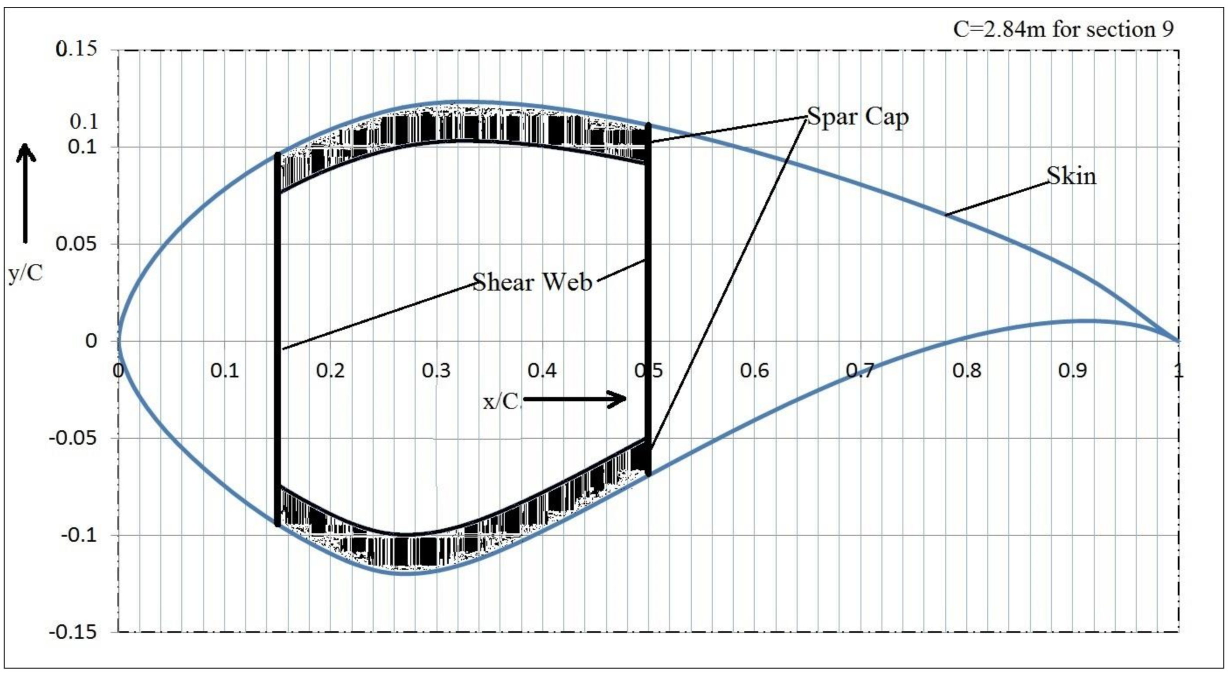

Figure 3.2: The S818 Airfoil Shape

3.5.2: Box spar

The box spar consists of thick spar caps at the top and bottom faces of the blade and shear webs connecting them throughout the length of the blade (Shown in Figure 3.2). For simplicity the whole box spar is assumed to be made of poly carbon fiber having the material properties shown in Table 3.1. Material properties such as structural rigidity, strength and light weight indicates that carbon fiber is ideal material for the spar cap. The spar caps have thickness of 8.4 cm at the root, 7 cm at the largest airfoil section and tapers to 2.3 cm at the blade end. The shear web has a thickness of 1.34 cm at the root, 1.2 cm at the largest section and tapers to 0.38 cm at the blade end.

3.5.3: Skin

A thin layer of glass fiber (the skin) is located surrounding the box spar. The tensile strength of glass fiber ensures necessary strength and structural integrity and also adds to the torsional resistance of the blade. The skin was modelled such that it has 7 mm thickness at the root, 6 mm at the largest airfoil section and it tapers to 1.7 mm thick at the end of the blade. The properties of the glass fiber used for the shell design are given in Table 1. For both of these materials, the objective was to introduce material properties that were similar to those used in actual turbine blade so that changes in blade behavior were representative of these geometries and materials.

3.6: Finite Element Modelling

For use in finite element analysis the entire blade is divided into elements. The model of the conventional length blade consists of 966 nodes together located at major locations in the elements. The nodes are joined together appropriately to form elements. There are 616 elements used to present the entire blade. The elements are all modelled as 8-noded brick elements and their material and structural properties were given accordingly (Table 3.1). In addition to that, the directions of the axes respective to the blade model are as shown in Figure 3.3. For further understanding a few of the sections that go into the model are shown below and the rest are explained in the appendix 1.

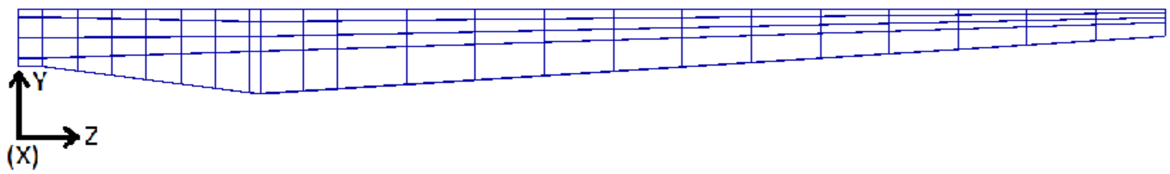

Figure 3.3: Axes of the Blade Model

Table 3.1: Material Properties of Poly-carbon fiber and Glass Fiber for Modeling Blade [23]

Material	**Graphite-polymer Composite**	**Glass-polymer Composite**
Density	1600 kg/m3	1900 kg/m3
E1	135 GPa	40.0 GPa
E2	10 GPa	8 GPa
E3	10 GPa	8 GPa
v23	0.6	0.5
v13	0.3	0.25
v12	0.3	0.25
G23	3.75 GPa	3 GPa
G13	5 GPa	4 GPa
G12	5 GPa	4 GPa

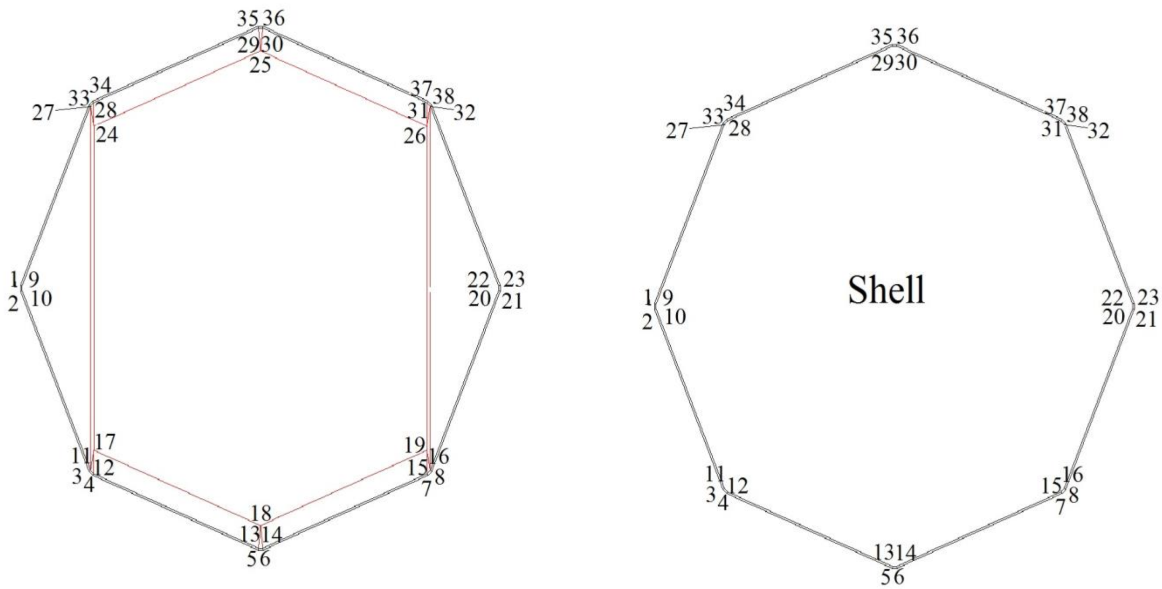

Figure 3.4: Section 1(Skin and Box spar)

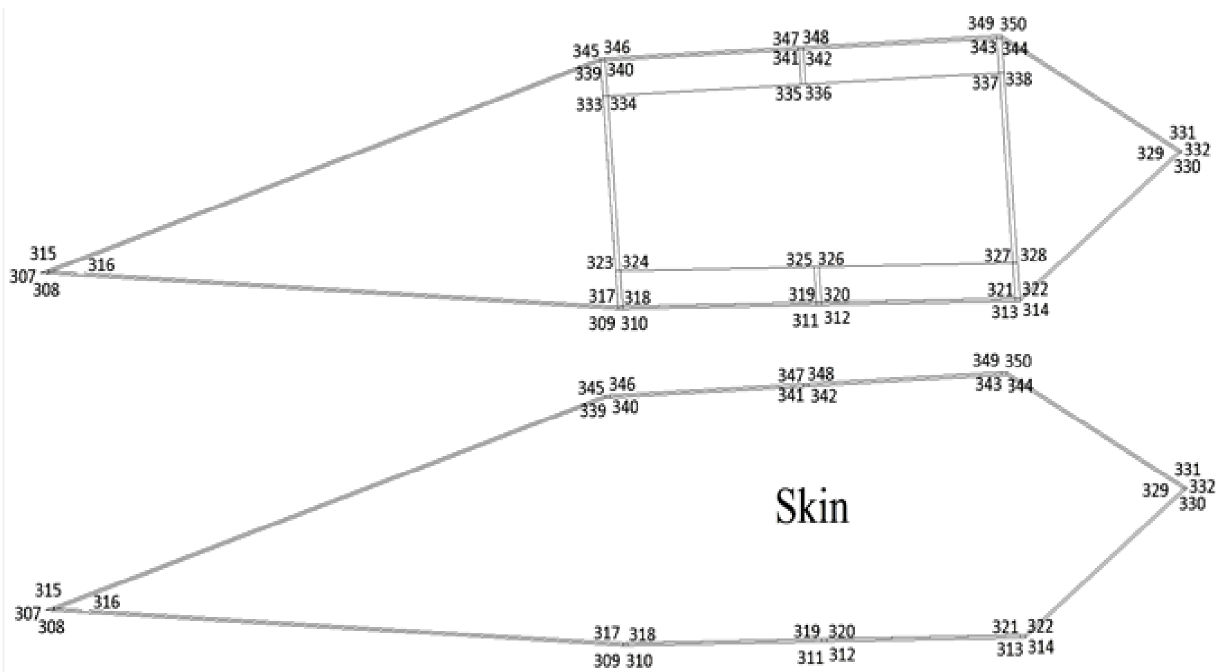

Figure 3.5: Representative node numbering for skin Section 9

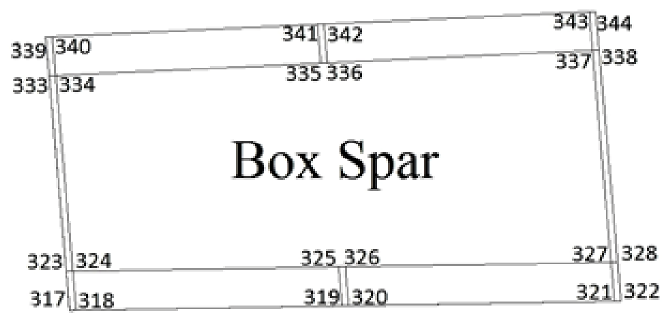

Figure 3.6: Representative node numbering for box spar of section 9

As mentioned earlier this is a very coarse mesh, hence the blade doesn't have the exact aerodynamic shape and allied details but serves the purpose to give us insight into the structural behavior of the blade and do comparative study between conventional blade and retracted blades. A figure of the entire modelled domain is shown in Figure 3.7.

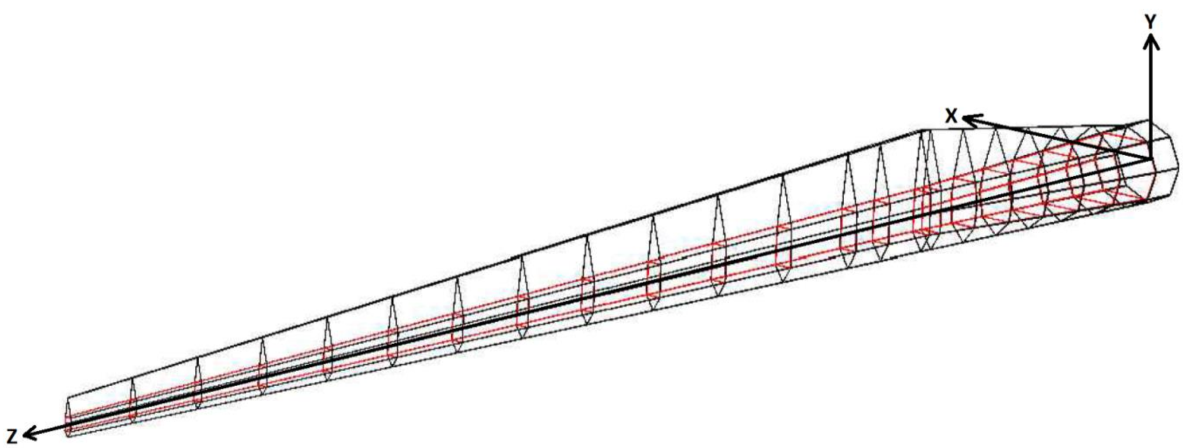

Figure 3.7: The entire modelled blade

3.6.1: Sections for the Finite Element Model

The blade has 23 sections spread across 33.25 m length of the blade. Each of these segments was modelled using single brick element. Although this is a very coarse discretization, it is not unreasonable to determine the bulk properties of the blade. This representation is shown in figure 3.8. The 1stand 2nd section are the same have circular cross- section, and every other section is different from the others either in size or shape.

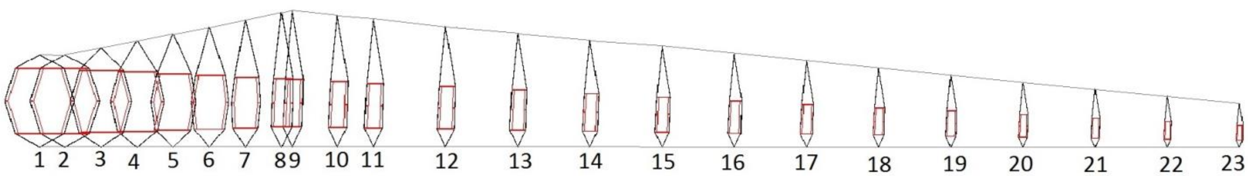

Figure 3.8: Longitudinal Profile of the modelled blade showing location of the sections

The distribution of nodes and elements for each section is as shown below in Table 3.2. As you can infer from the table the spacing of the sections are not the same. The section spacing is around 1 m for the first few sections, since they are transitioning from hexagonal cross-section to the airfoil section. Then gradually the spacing becomes 2 m since the cross-sectional shape doesn’t change much.

The next major step in modelling is fixing the appropriate loading values for analysis. They are explained in section 4.1 of Chapter 4.

Table 3.2: Nodes, Element and Chord Length details of various Sections in the Blade Model

Section	Distance from Section1	Number of nodes	Number of Elements	Chord Length (meters)
1	0.0	38	28(connecting Section 1 and 2)	1.925
2	0.7	38	28	1.925
3	1.7	38	28	2.070
4	2.7	38	28	2.215
5	3.7	38	28	2.360
6	4.7	38	28	2.505
7	5.7	38	28	2.650
8	6.7	40	28	2.800
9	7.0	44	28	2.840
10	8.25	44	28	2.747
11	9.25	44	28	2.674
12	11.25	44	28	2.528
13	13.25	44	28	2.382
14	15.25	44	28	2.236
15	17.25	44	28	2.090
16	19.25	44	28	1.944
17	21.25	44	28	1.798
18	23.25	44	28	1.652
19	25.25	44	28	1.506
20	27.25	44	28	1.360
21	29.25	44	28	1.214
22	31.25	44	28	1.068
23	33.25	44		0.925

3.7: The Retracted Blades

As informed above the aim of the study is to compare the static deflection and fundamental frequency of vibration properties between conventional blade and various retracted positions of extendable wind turbine blade.

For simplicity the comparison to conventional blade is done for the 5 retracted positions given below. The conventional blade length is named as blade 1, the first retracted blade position is named as blade 2 and so on. Figure 3.9 shows a comparison of the various retracted blades and Table 3.3 lists out the effective length of blades when they are retracted.

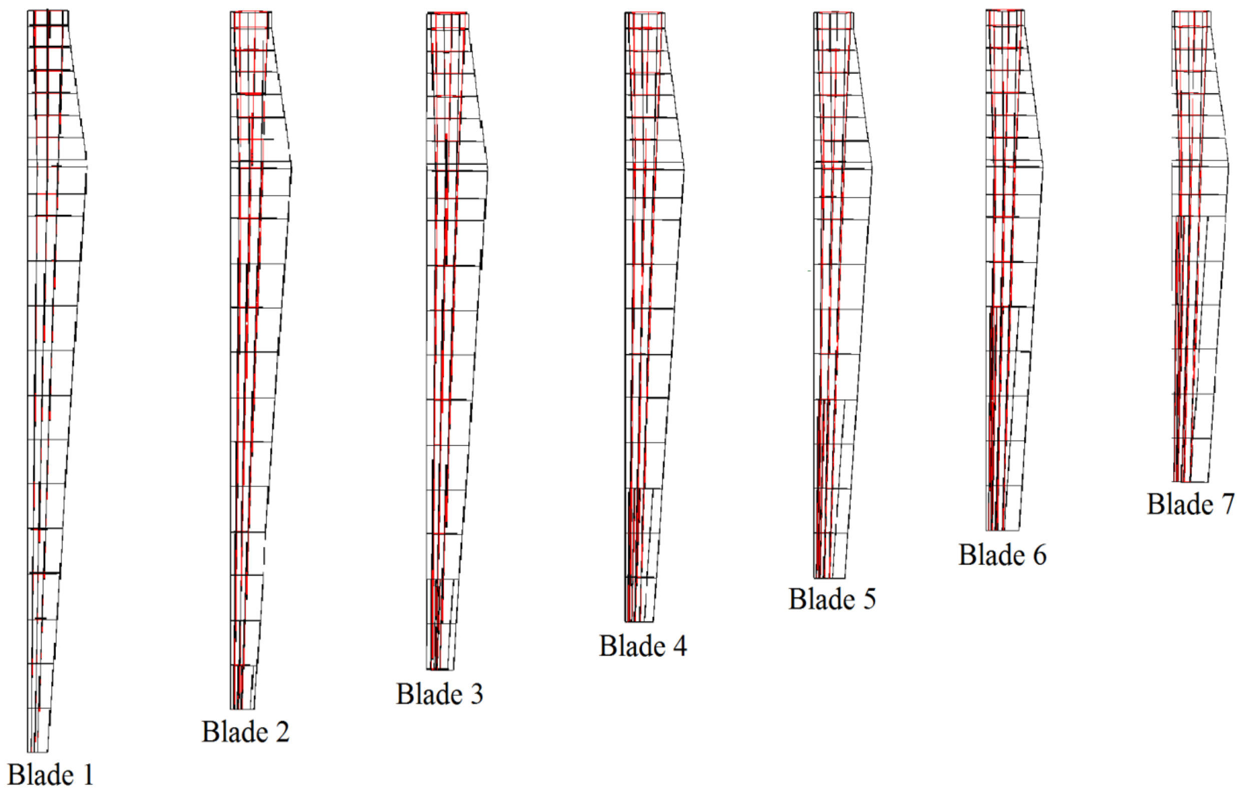

Figure 3.9: Various Blade lengths for comparison

Table 3.3: Retracted Length of Blades

Blade No.	Retracted Blade Length	Number of Nodes	Number of Elements
1	33.25 (Full Blade length)	966	616
2	31.25	922	588
3	29.25	878	560
4	27.25	834	532
5	25.25	790	504
6	23.25	746	476
7	21.25	702	448

The different blades are not retracted positions of a same retractable blade, but blades of different retracted blade length. Figure 3.10 is a portion of the Blade 2. The diagram clearly shows the Section at which the blade retracts. Portion of the blade between section 22 and 23 retract here at Section 22.

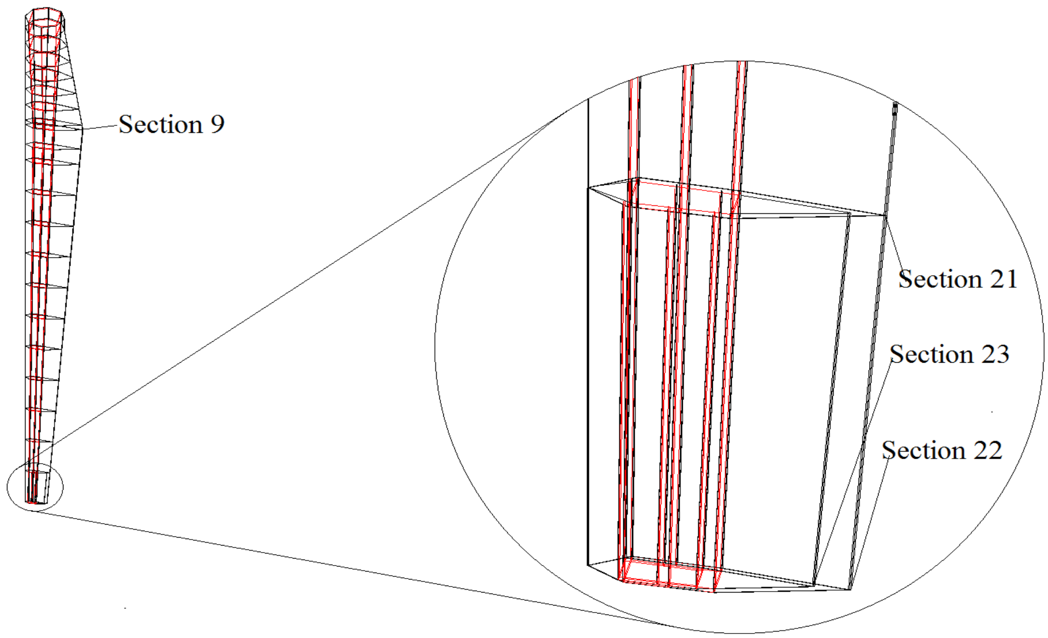

Figure 3.10: Portion of Blade 2

In Blade 2 the portion between section 23 and 21 retracts at section 21 inwards. And so on for the rest of the sections. For analysis the mass of the retracted portion of the blade is treated differently. We distribute the entire mass of the retracted portion of the blade on the box spar of the portion it retracts into. In the case of blade 2 we calculate the mass of the retracted portion of blade (i.e. portion between section 23 and 22 and add the mass evenly on to the box spar between section 22 and 21. This ensures that the blade is treated for analysis as close to the practical scenario. Similarly in blade 3 the mass of blade between 23 and 21 is evenly distributed in the box spar between 21 and 19, and so on.

CHAPTER 4: ANALYSIS

4.1: Calculation of Static Deflection

In this chapter we study the quasi-static deflection of the turbine blade under a combined wind load along with the dead load of the blade. This is accomplished by analyzing the finite element model described earlier using FORTRAN. Therefore after the modelling explained in the previous chapter, the next step is to estimate the loading on the blade.

4.1.1: Wind Loading

The study here is to relate the behavior of the blades when subjected to wind loading under fully extended and then partially extended positions. We consider a reasonable wind speed of 11m/s [24] for calculation of wind force and hence the wind loading on the blade.

As the blade rotates, when its position is below the hub, the maximum wind load acts at the root of the blade. And when its position is above the hub height, maximum wind load acts at the tip of the blade. So clearly the wind load varies in magnitude through the length of the blade. But for simplicity and since the scope of the study is to comparison between the extendable and non-extendable blade, we assume constant wind speed of 11 m/s from the root to the tip of the blade.

Knowing the wind velocity we can compute from the wind pressure using the Bernoulli's equation for pressure equilibrium.

$$P = \frac{1}{2}\rho v^2,$$

Here,

P=Wind Pressure

ρ= Density of air=1.2754 kg/m^3

v=Incident wind velocity

As an intermediate procedure, we compute the effective areas for each node, whose loads acts at the corresponding node. Hence knowing the area for each node and the wind pressure we compute the wind load for each node, and are also made to act in the positive x-direction. In equation 3.3, the force vector includes all kind of loading acting on the blade. Each term in the vector consists of body force and surface loading acting on the corresponding element. So the wind loading is accounted for in our analysis as the surface terms in the Force Vector of Equation 3.3. Effectively this comprises the wind loading on the beam.

4.1.2: Dead Load

The dead load is calculated for each element and made to act independently for each element, essentially acting as a uniformly distributed load over the blade. And mass varies depending on the element size and the kind of material. It is acting in the positive x-direction. In Equation 3.3 this is accounted for, in the force term as the body force.

4.1.3: Method of Computing Deflection

Section 3.1and 3.2 in Chapter 3 explains in detail how the deflections are computed using Finite Element Analysis. It explains how the stiffness matrix and force vectors are formed and how the displacement vector is calculated using Equation 3.5. But for multiple elements, an intermediate step is essential. The stiffness matrix for each of the elements is assembled to form Global Stiffness Matrix, and the vectors are assembled to form Global Vectors. Hence the displacements are calculated using the Global Stiffness Matrix and Global Force Vector.

And once we analysis the done, the output consists of displacement occurring for each node. From the 966 displacement values, a set of nodes are selected such that they all fall in a straight line along the length of the beam. The nodes selected are marked in the figure below. And since the loading is flapwise (in the x-direction), we consider the displacements also in the x-direction.

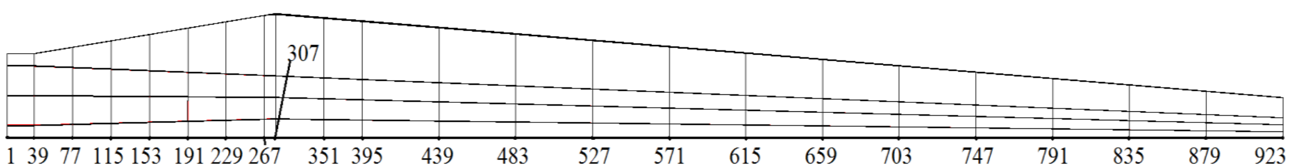

Figure 4.1: Coordinates selected to plot static displacement

4.2: Calculation of Stresses

Stresses were calculated after computing the static displacement for node. But in FEA the stresses are computed at the gauss points, so the nodal displacements cannot be directly used to calculate stresses. Hence as an intermediate procedure displacements are computed at the gauss points first. Then equation 3.2 is employed to calculate the longitudinal stress (σ_{xx}) and transverse stress (σ_{xz}). In our study since the longitudinal axis is the ‘z axis’ and not ‘x axis’, the longitudinal stresses are denoted as, σ_{zz} and the transverse stress is denoted the same.

After analysis the output would contain (number of nodes*8) values. (Refer Table 3.3 for number of nodes for each blade). Then the beam is separated into portions. For example portion of blade between section 1 and section 2 would be portion 1.The portion of blade between section 2 and section 3 would be portion 2, and so on. And each portion would contain 28 elements (28*22=616 elements). So, there would a total of 22 portions (Table 4.1). From the output, the stresses are ordered portion-wise and maximum stress is calculated for each portion. And the stresses would be located at the center of each element. The resultant graph should variation of stresses are plotted and explained in Chapter 5. For additional reference Figure 4.2 shows portions of the blade.

Table 4.1: Portions Details

Portion Number	Set of Elements Included	Distance to center of portion
1	1-28	0.35
2	29-56	1.20
3	57-84	2.20
4	85-112	3.20
5	113-140	4.20
6	141-168	5.20
7	169-196	6.20
8	197-224	6.85
9	225-252	7.625
10	253-280	8.75
11	281-308	10.25
12	309-336	12.25
13	337-364	14.25
14	365-392	16.25
15	393-420	18.25
16	421-448	20.25
17	449-476	22.25
18	477-504	24.25
19	505-532	26.25
20	533-560	28.25
21	561-588	30.25
22	589-616	32.25

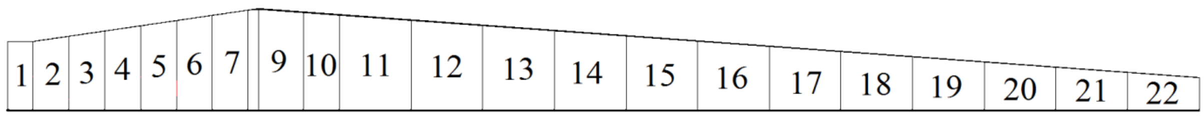

Figure 4.2: Portions of the blade

4.3: Calculation of Shear Force and Bending Moment

Since the retracted blades have two blades jointed together, design of the joint is crucial. Hence the shear force and bending moment at the end of the root blade are essential for design purposes. They are tabulated in section 5.1.4 and 5.2.4, in Chapter 5.

4.4: Calculation of Vibrational Frequency And Modes

Initial details regarding formation of the weak form equation (Equation 3.6) and assembly of matrices are explained in section 3.1, 3.3 and 4.1.2. After assembling the Global Matrices and Vectors, Fortran Program was used to solve for the fundamental frequency and modes of vibration by Generalized Eigen Value Problem Method. The lowest non-zero value from the calculated array of Eigen Value is the fundamental frequency, and the non-zero vectors from the Eigen vector solution are the modes of vibration of the blade. We consider the first six modes of vibration for comparison. Section 5.3 sums up the results for vibrational modes and frequency for all the blades.

CHAPTER 5: RESULTS

5.1: Load Case 1(Wind Load Only)

5.1.1: Static Deflection

Static deflections for wind load alone were calculated for all the blades, and a condensed graph of the same, is represented below.

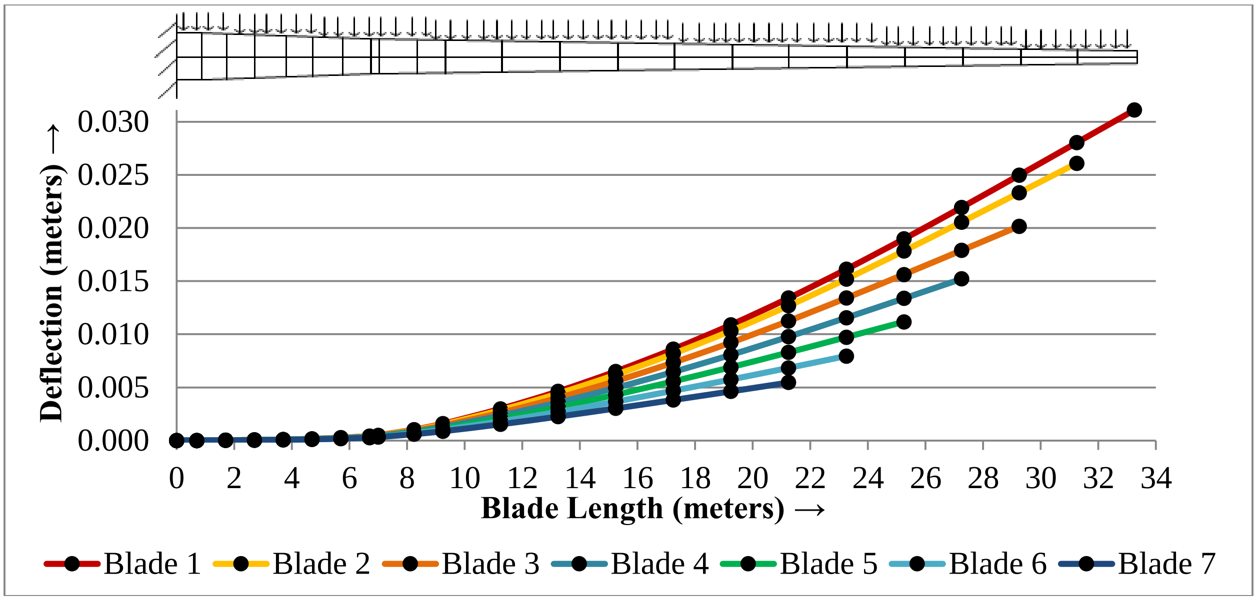

Figure 5.1: Comparison of Static Deflections (W only)

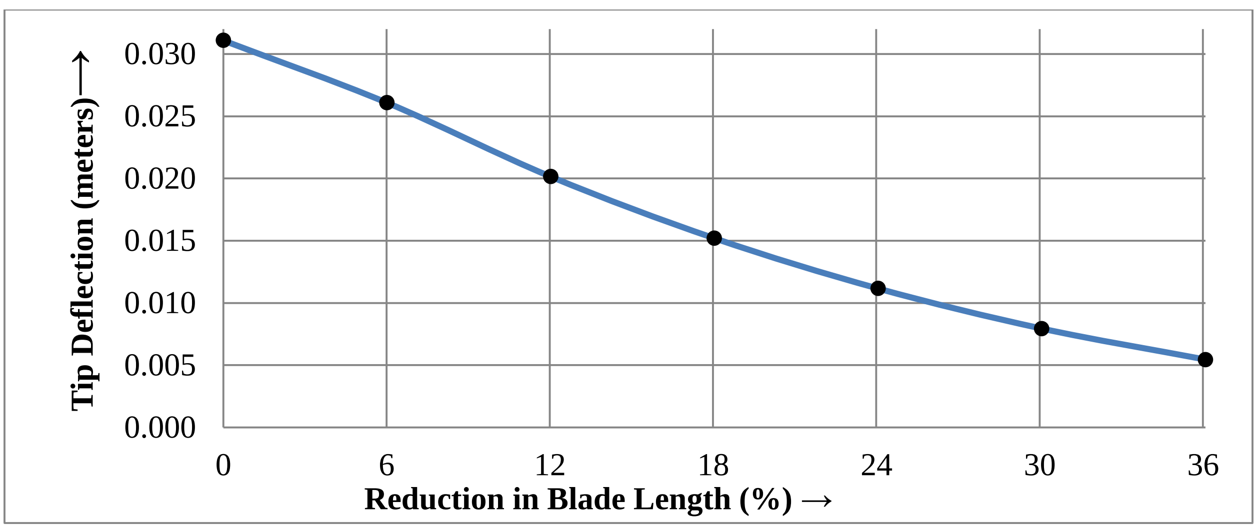

Figure 5.2: Deflection for Percentage Reduction in Blade Length (W only)

5.1.2: Stresses

Figure 5.5 shows maximum longitudinal stress in tension for all the blades. For all cases it was seem that stresses peak at the 8th portion (about 7 m from the root of the blade).

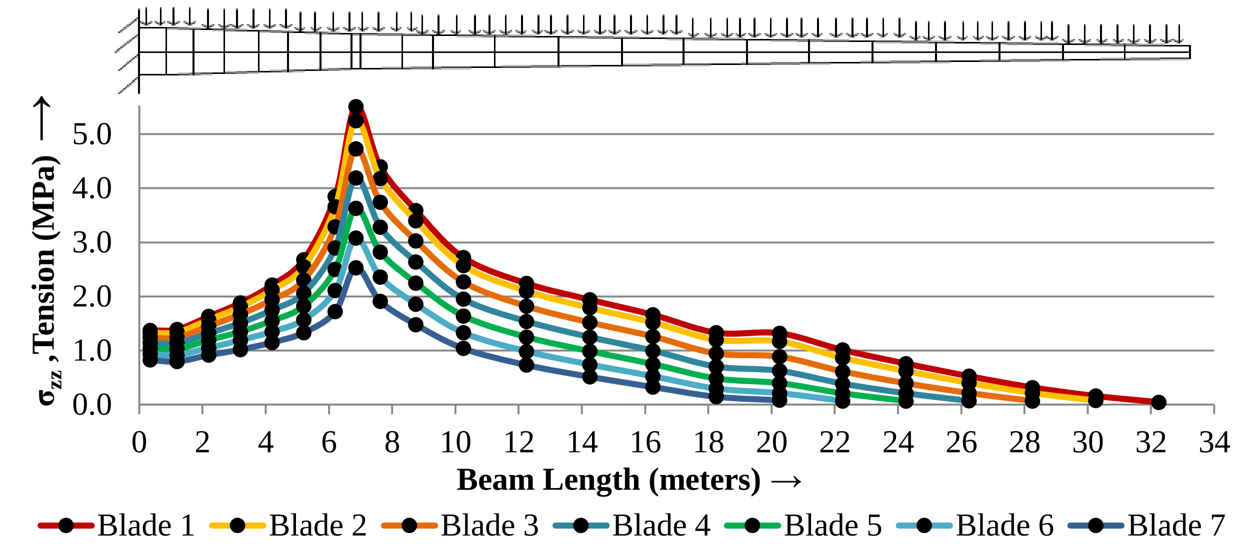

Figure 5.3: Comparison of Maximum σ_{zz} in Tension (W only)

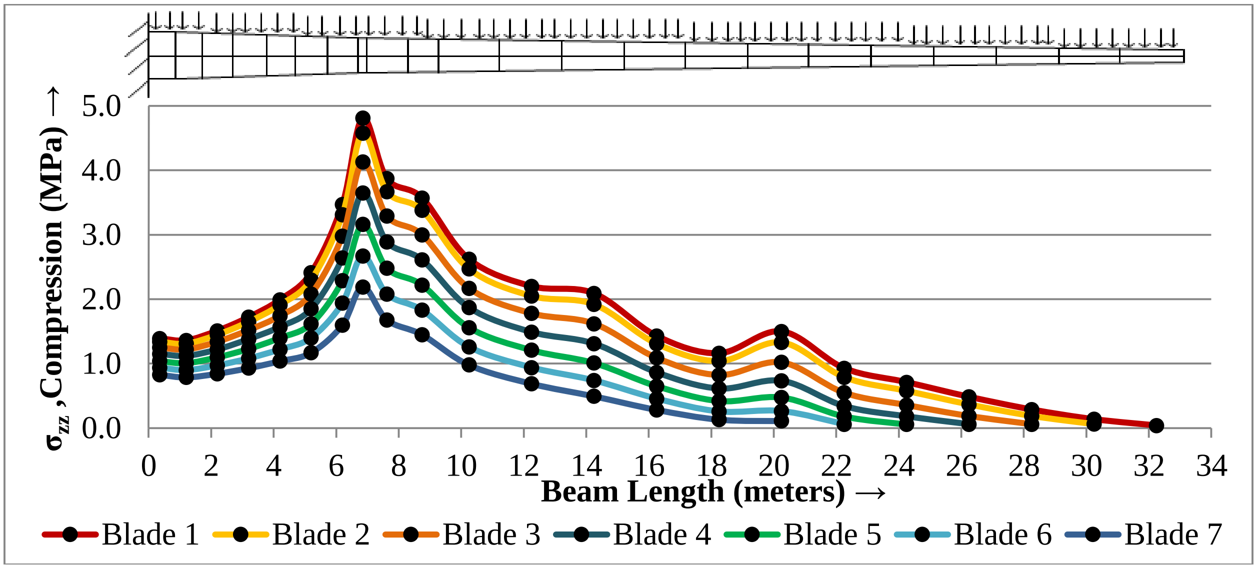

Figure 5.4: Comparison of Maximum σ_{zz} in Compression (W only)

Furthermore Figures 5.7 and 5.8 shows maximum stress for various blades (in tension and compression) for longitudinal and transverse stresses respectively.

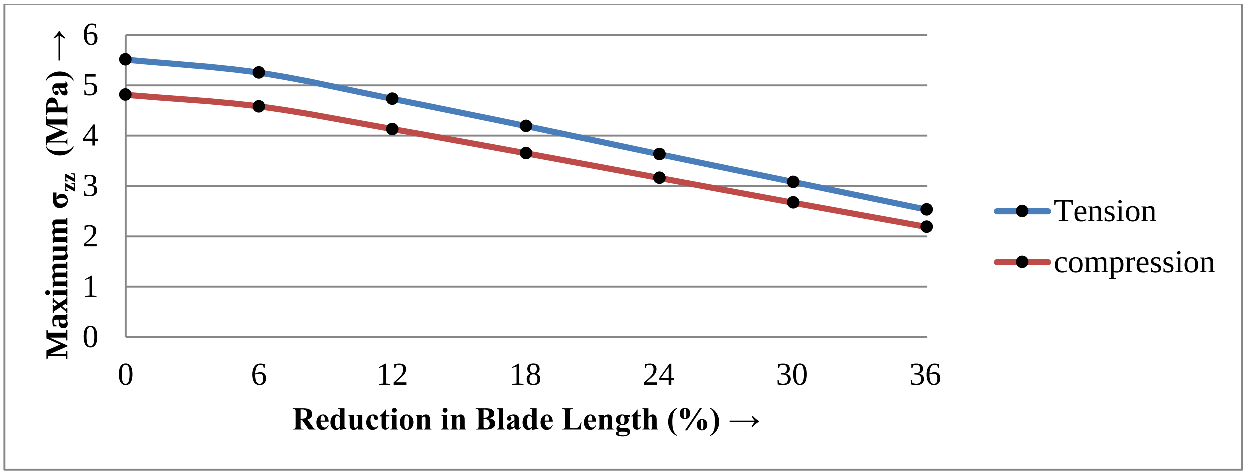

Figure 5.5: Maximum σ_{zz} for Percentage Reduction in Blade Lengths (W only)

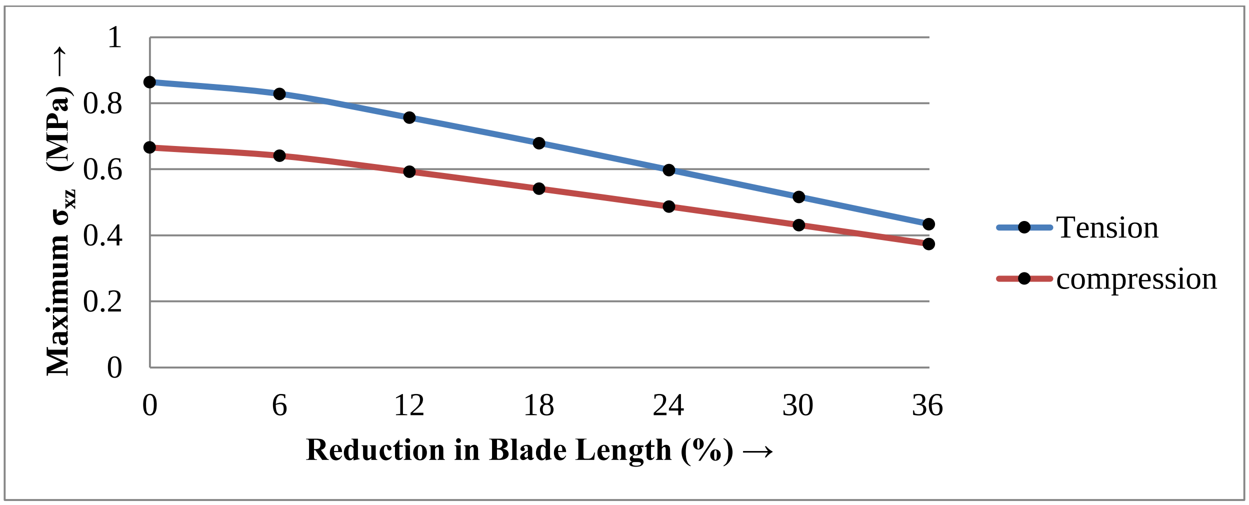

Figure 5.6: Maximum σ_{xz} for Percentage Reduction in Blade Lengths (W only)

Here we could see that there is a linear decrease in stresses for all the retracted blades. The slight non-linear behavior is due to inclusion of the full length blade to the data set.

5.1.3: Shear Stress and Bending Moment at the End of Root Blade

Table 5.1: Shear Force at the point of retraction (W only)

Blade	Blade 1	Blade 2	Blade 3	Blade 4	Blade 5	Blade 6	Blade 7
Shear Force (N)	79.93	251.49	446.5	664.93	906.75	1172.01	1460.72
Bending Moment (kN-m)	77.11	74.45	69.08	63.38	57.43	51.32	45.16

5.2: Load Case 2 (Dead Load + Wind Load)

5.2.1: Static Deflection

Now for second load case the deflections for various blades are as shown below.

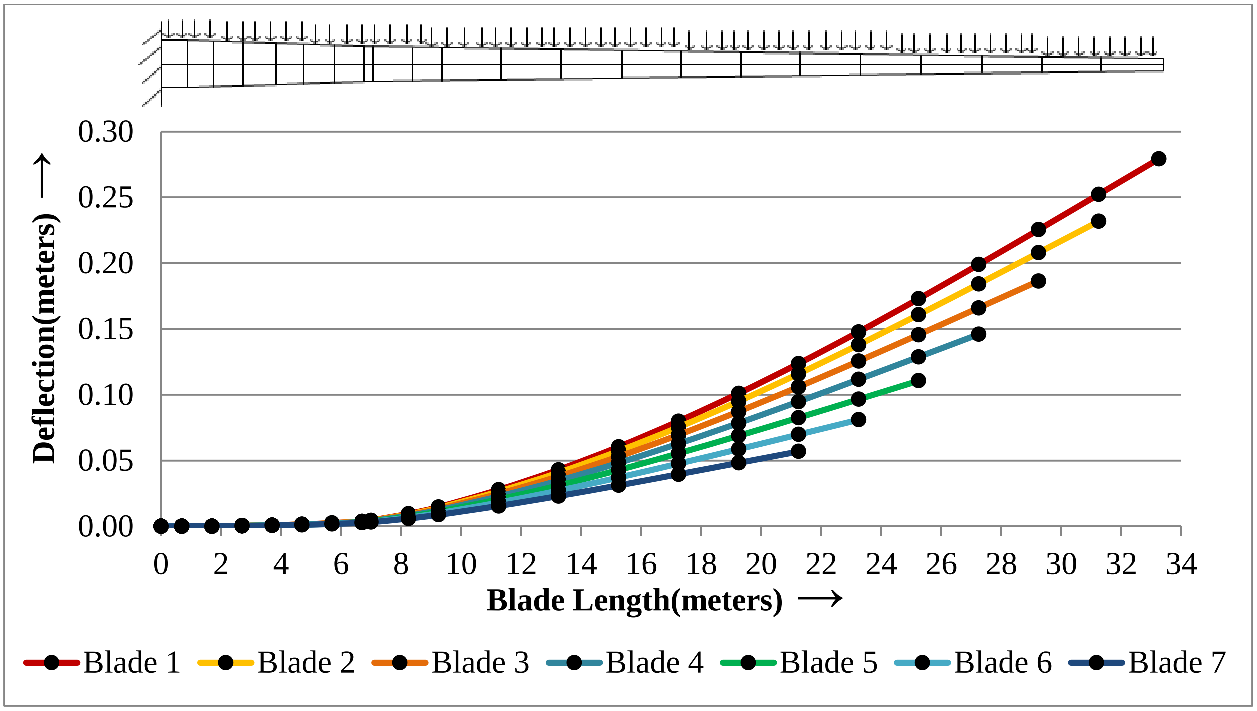

Figure 5.7: Comparison of Static Deflections (W+D)

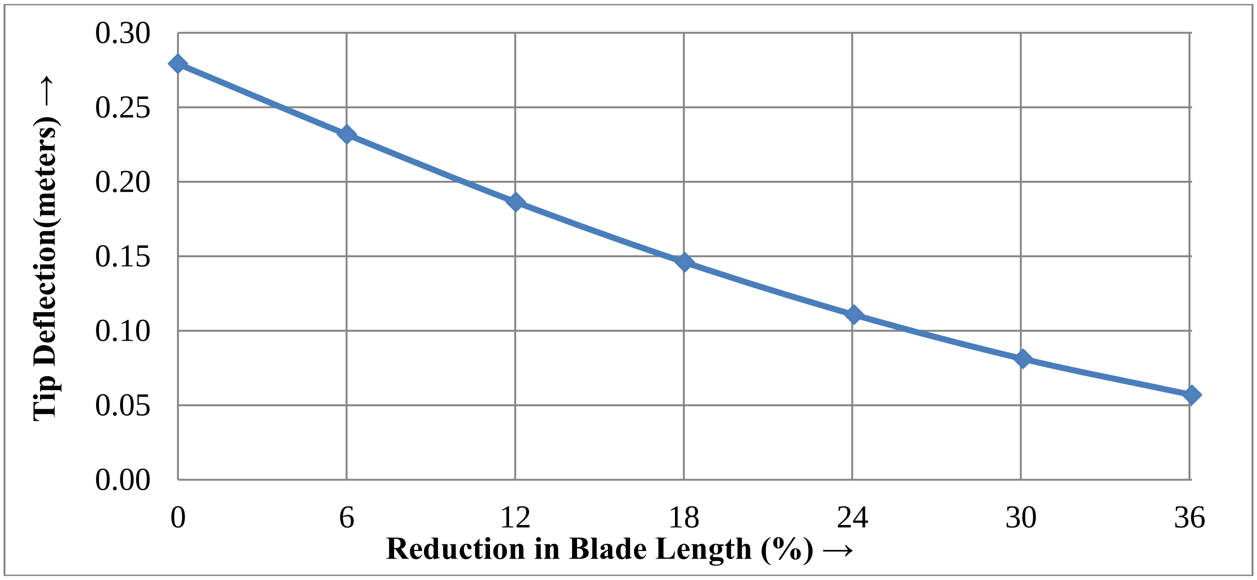

Figure 5.8: Deflection for Percentage reduction in Blade Length (W+D)

5.2.2: Stresses

Similar to the previous load case the peak stresses are at the same location.

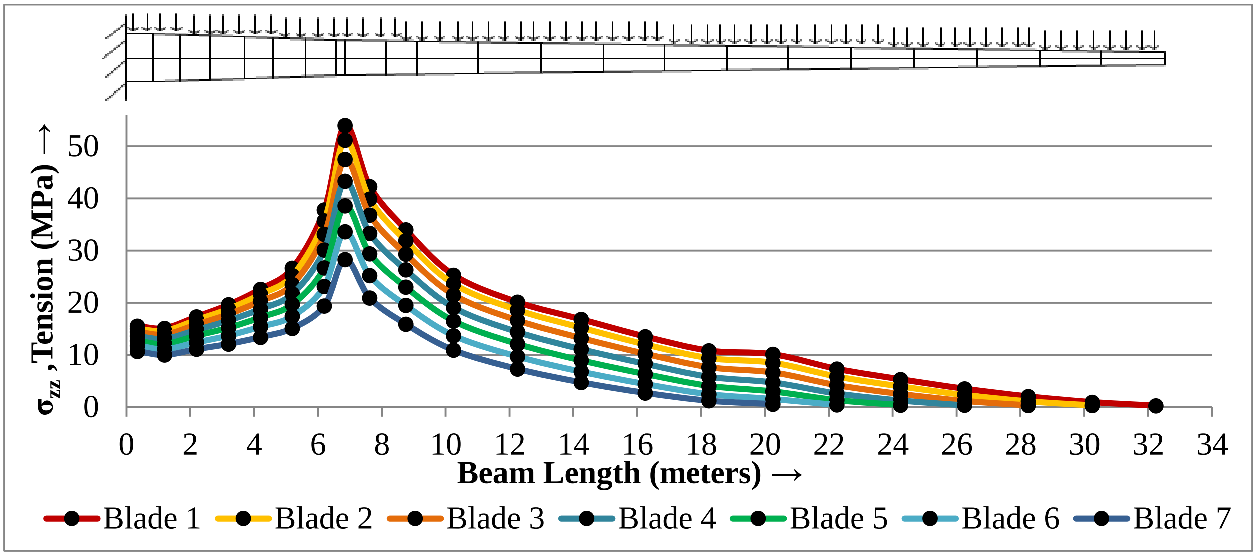

Figure 5.9: Comparison of Maximum σ_{zz} in Tension (W+D)

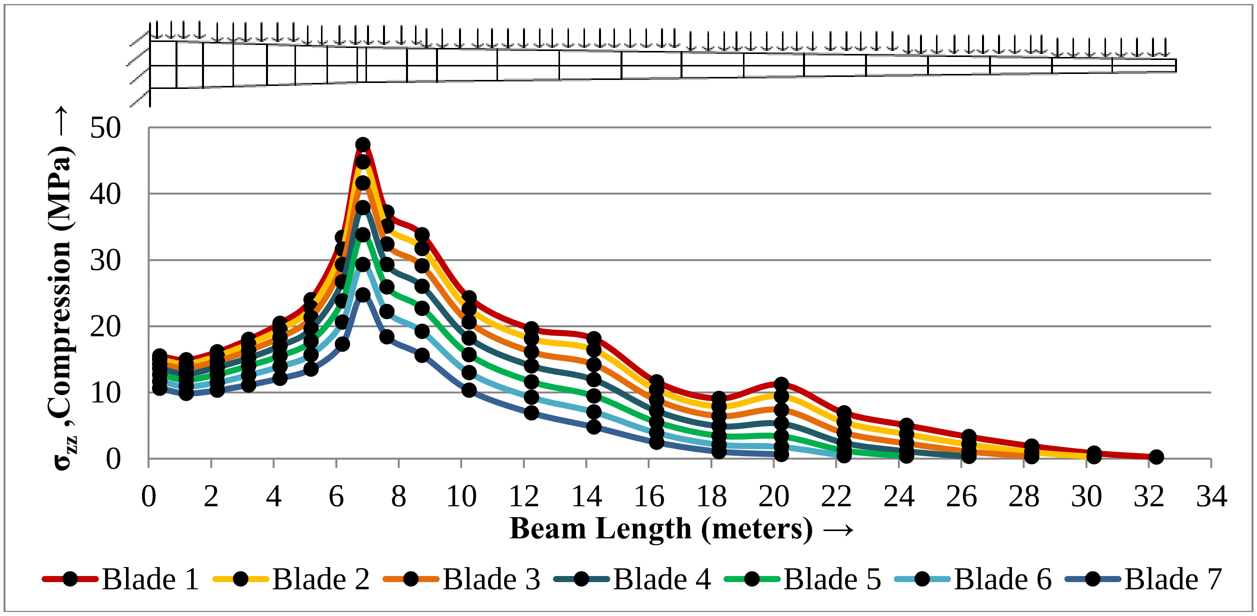

Figure 5.10: Comparison of Maximum σ_{zz} in Compression (W+D)

Furthermore, Figures 5.11 and 5.12 shows how much stress reduces when retractable blades are employed instead of conventional blades.

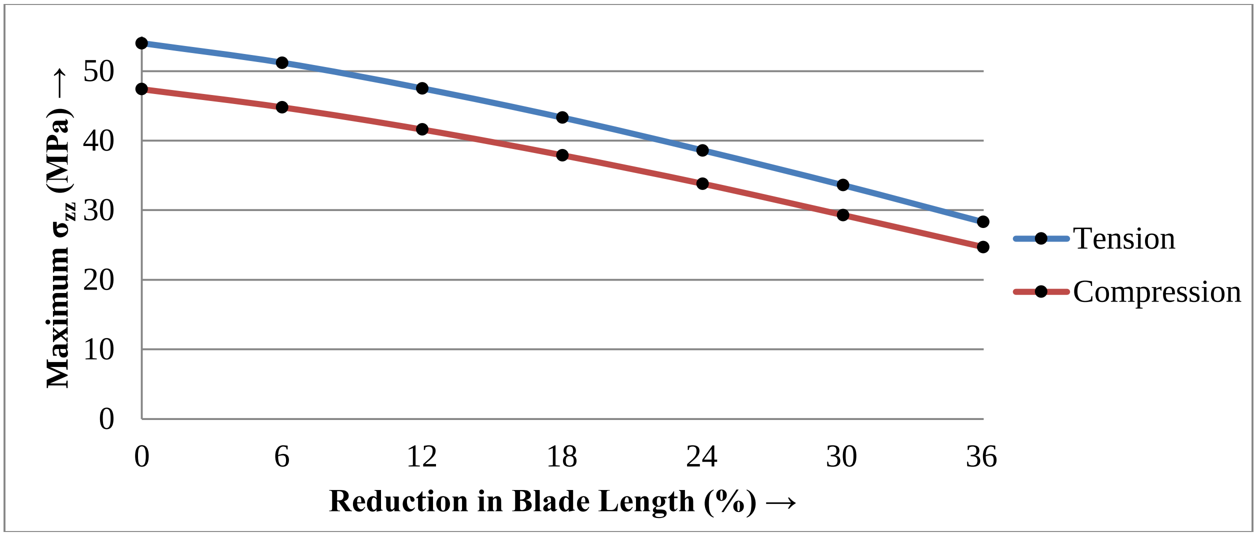

Figure 5.11: Maximum σ_{zz} for percentage reduction in Blade Lengths (W+D)

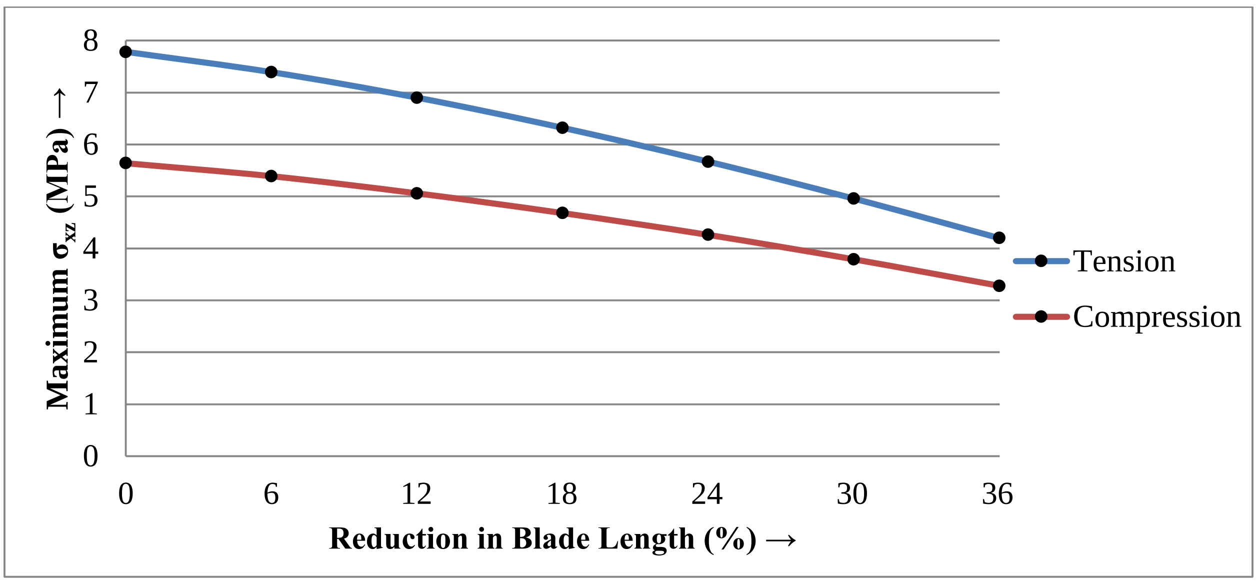

Figure 5.12: Maximum σ_{xz} for percentage reduction in Blade Lengths (W+D)

5.2.3: Shear Stress and Bending Moment at the End of Root Blade

Table 5.2: Shear Force at the point of retraction (W only)

Blade	Blade 1	Blade 2	Blade 3	Blade 4	Blade 5	Blade 6	Blade 7
Shear Force (N)	79.93	318.79	602.30	933.23	1314.40	1748.91	2239.52
Bending Moment (kN-m)	620.06	618.74	613.94	604.26	588.06	563.46	528.38

5.3: Fundamental Frequency of Vibration

This section encompasses the results for vibrational analysis of the blades. Initially the results for the Blade 1 are tabulated in the table below. Then the vibrational mode and frequency of the remainder blades are contrasted with that of Blade 1.

5.3.1: Vibrational Mode and Frequency of Blade 1

The vibrational modes and frequencies for Blade 1 are tabulated in Table 5.3. And the various mode shapes are as shown in figures 5.15 to 5.20.

Table 5.3: Vibrational Modes and Frequencies of Blades 1

Mode number	Vibration Mode	Vibration Frequency(Hz)
1	Flapwise	1.408
2	Edgewise	2.097
3	Flapwise	5.410
4	Edgewise	7.296
5	Flapwise	12.521
6	Torsion	14.628

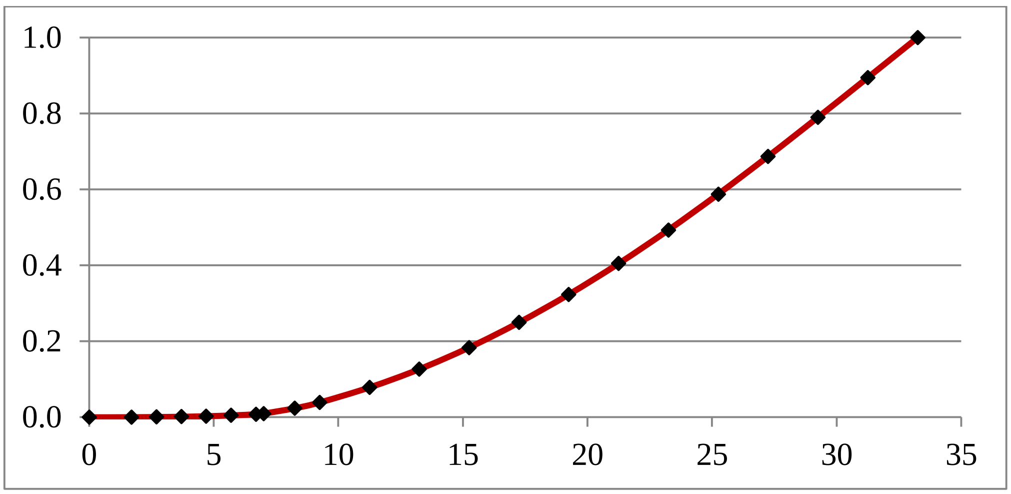

Figure 5.13: The First Modal Shape (Blade 1)

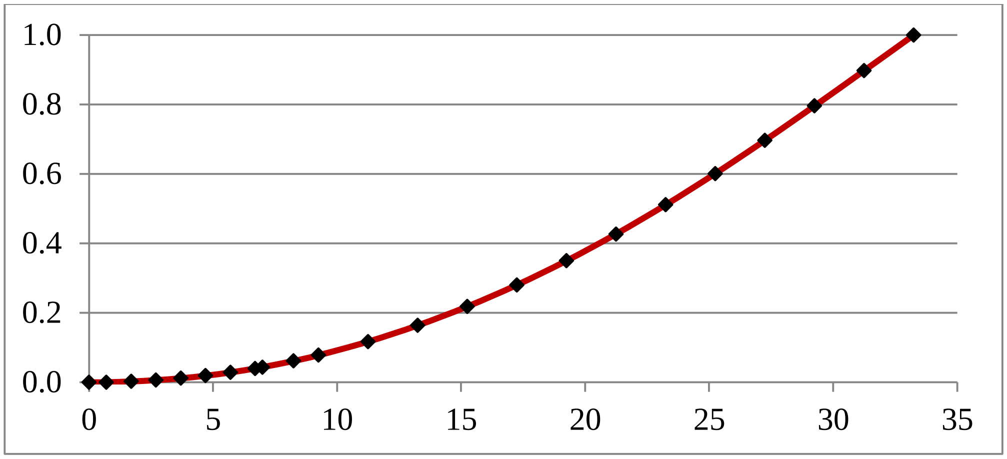

Figure 5.14: The Second Modal Shape (Blade 1)

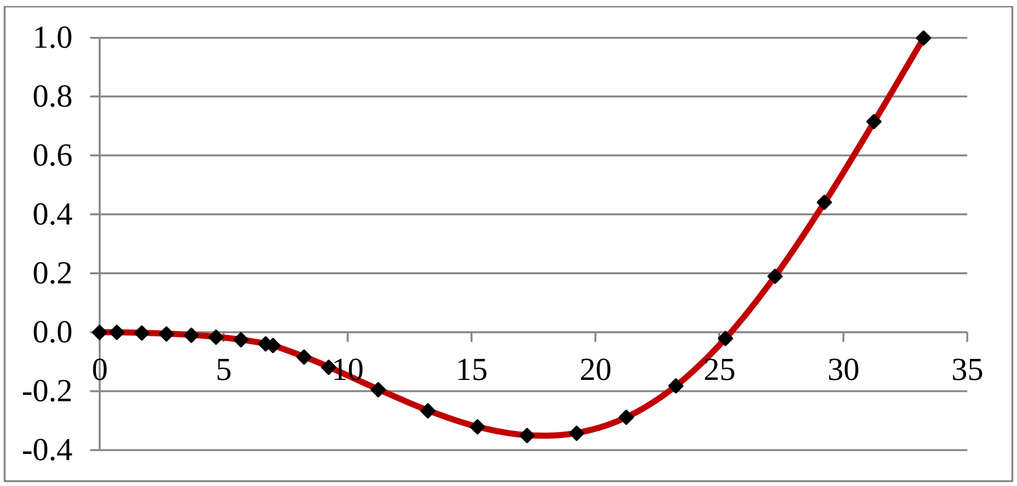

Figure 5.15: The Third Modal Shape (Blade 1)

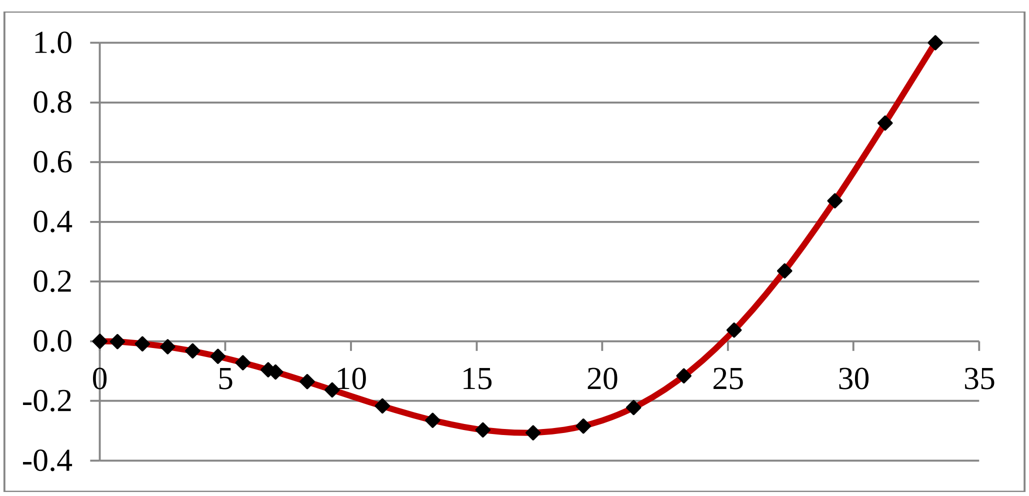

Figure 5.16: The Forth Modal Shape (Blade 1)

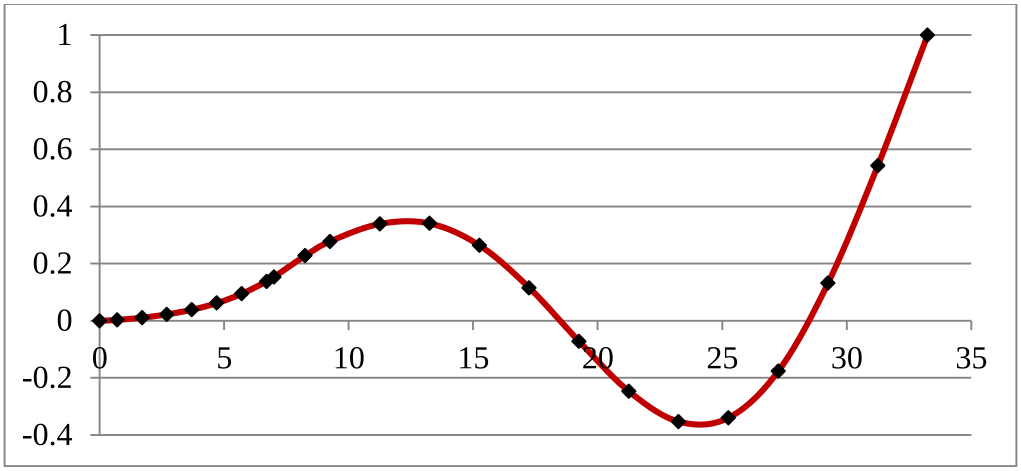

Figure 5.17: The Fifth Modal Shape (Blade 1)

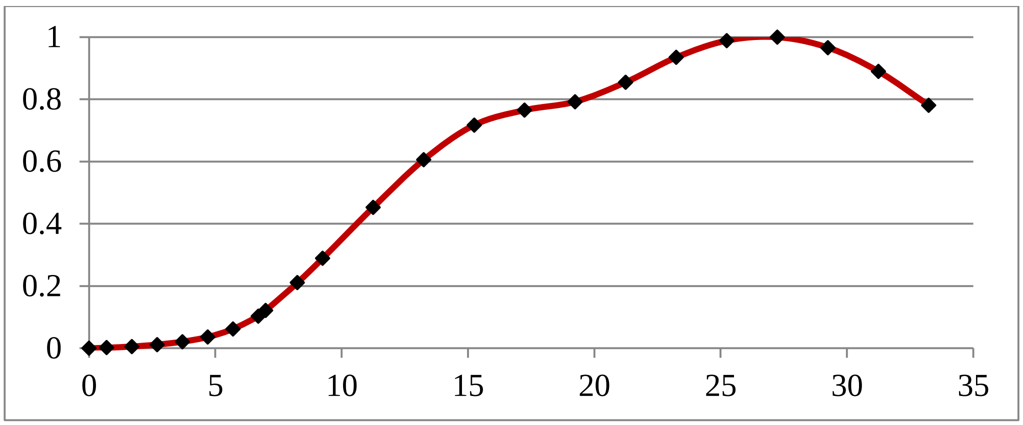

Figure 5.18: The Sixth Modal Shape (Blade 1)

5.3.2: Vibrational Mode and Frequency of other blades with Blade 1

Table 5.4 is a comparison of vibrational frequencies of all the blades and Table 5.5 sums up the first six vibrational modes of all the blades.

Table 5.4: Vibrational Frequencies of Various Blades

Mode No.	**Vibration Frequency(Hz)**						
	Blade 1	Blade 2	Blade 3	Blade 4	Blade 5	Blade 6	Blade 7
1	1.408	1.519	1.664	1.851	2.095	2.418	2.857
2	2.097	2.248	2.441	2.683	2.990	3.384	3.895
3	5.410	6.097	6.959	8.034	9.372	11.037	13.099
4	7.296	8.198	9.306	10.669	12.350	14.438	17.045
5	12.521	14.087	15.132	15.552	16.087	16.777	17.680
6	14.628	14.854	15.997	18.218	20.821	23.840	27.420

Table 5.5: Vibrational Modes of Various Blades

Mode No.	Blade 1	Blade 2	Blade 3	Blade 4	Blade 5	Blade 6	Blade 7
1	Flapwise	Flapwise	Flapwise	Flapwise	Flapwise	Flapwise	Flapwise
2	Edgewise	Edgewise	Edgewise	Edgewise	Edgewise	Edgewise	Edgewise
3	Flapwise	Flapwise	Flapwise	Flapwise	Flapwise	Flapwise	Flapwise
4	Edgewise	Edgewise	Edgewise	Edgewise	Edgewise	Edgewise	Edgewise
5	Flapwise	Flapwise	Torsion	Torsion	Torsion	Torsion	Torsion
6	Torsion	Torsion	Flapwise	Flapwise	Flapwise	Flapwise	Flapwise

An interesting fact we can notice is that vibrational modes of Modes 5 and 6, switch from Blade 3 onwards. In addition, Figures 5.21 to 5.26 gives a comparison of the modes of vibration of Blade 1, 4 and 7.

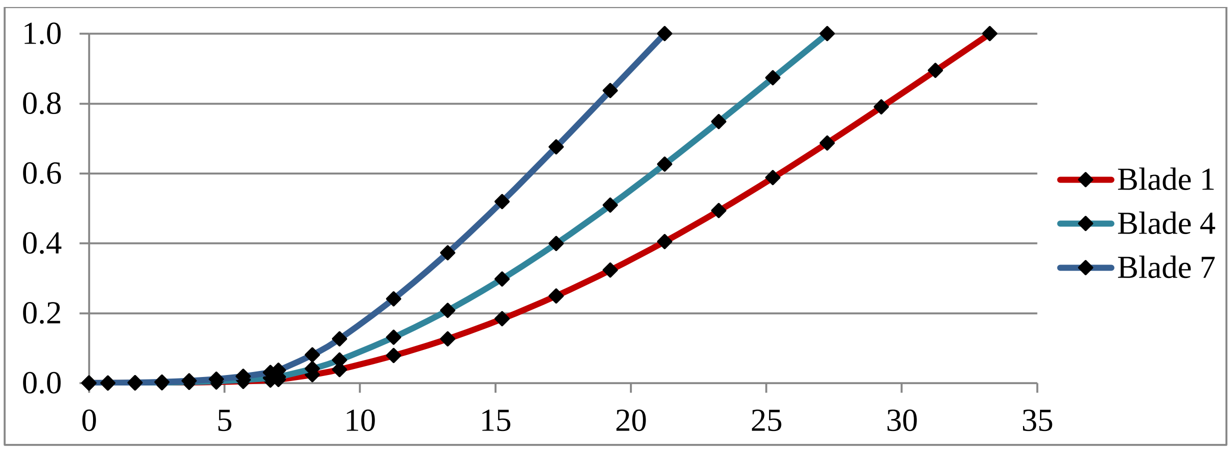

Figure 5.19: The First Modal Shape

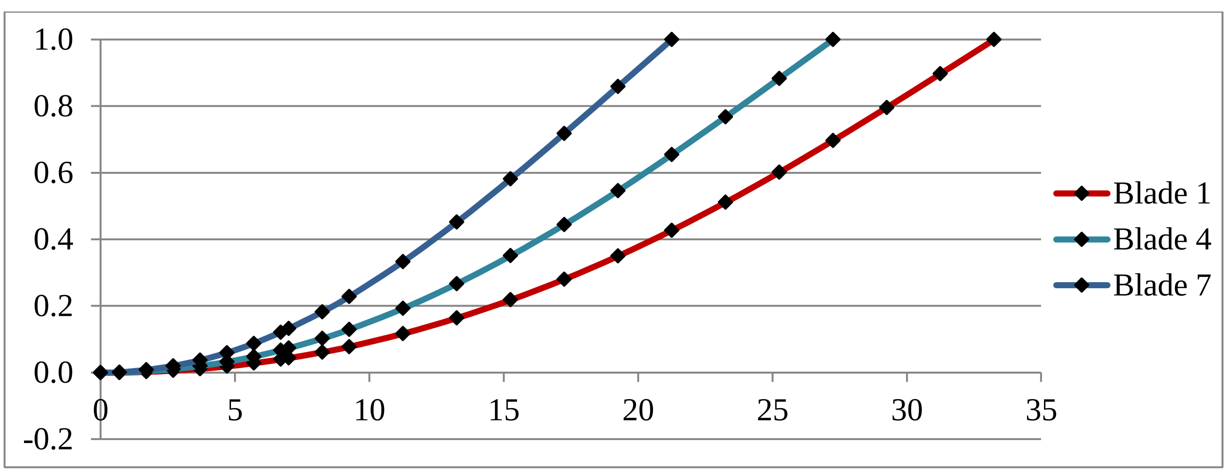

Figure 5.20: The Second Modal Shape

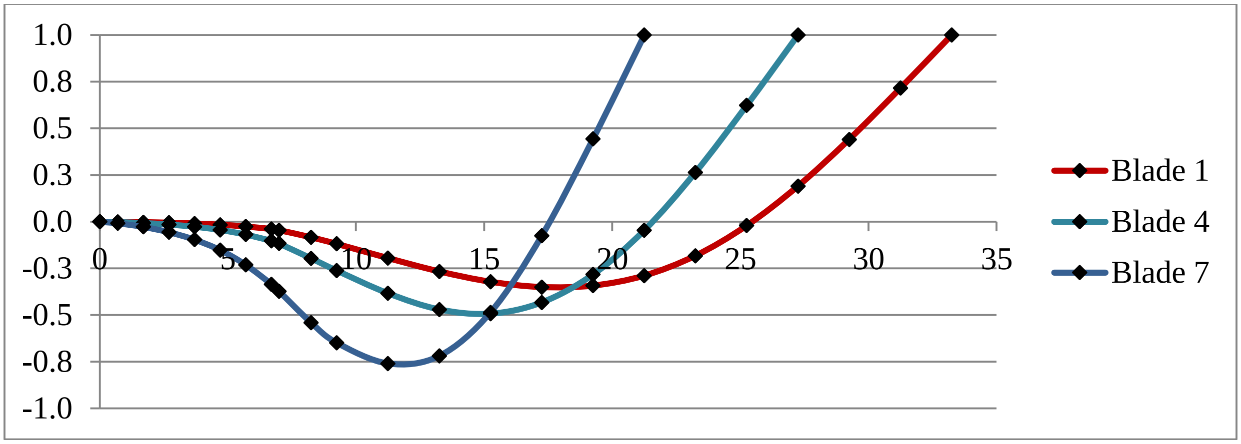

Figure 5.21: The Third Modal Shape

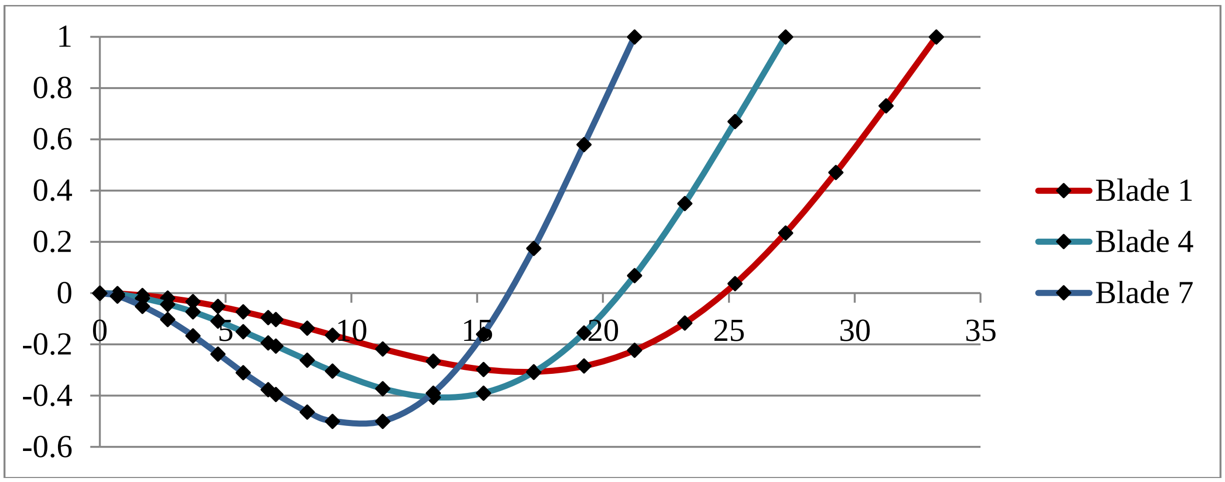

Figure 5.22: The Forth Modal Shape

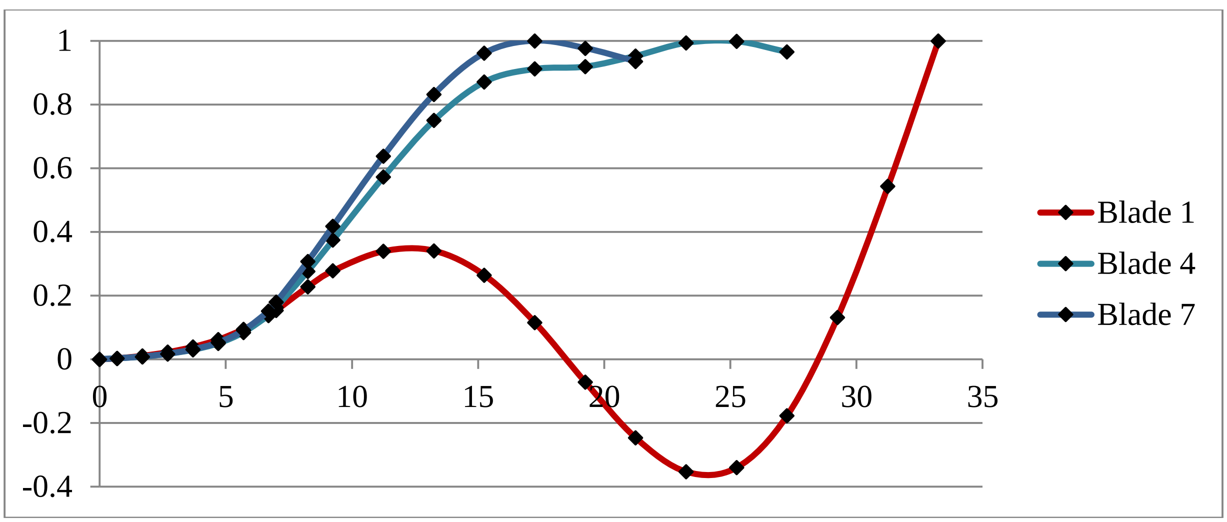

Figure 5.23: The Fifth Modal Shape

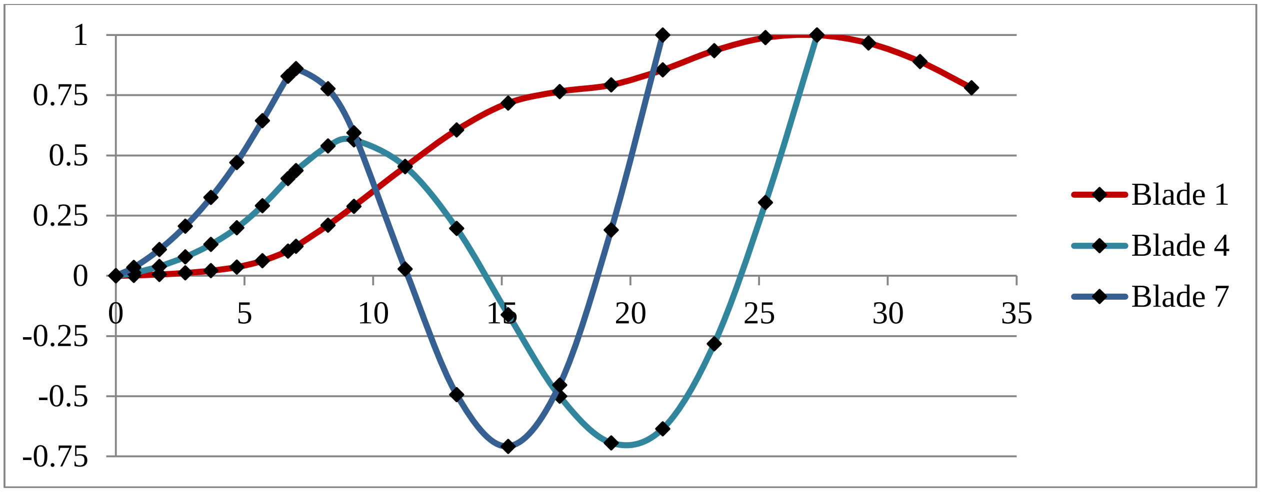

Figure 5.24: The Sixth Modal Shape

5.4: Validation of the Finite Element Model

The Finite element model in our study was also verified with that of earlier studies and the result is as shown below. Material details and loading conditions were considered from the reference studies [24][25][26] and were plugged into the FE Model of this study and the results were compiled in a similar manner.

Table 5.6: Comparison of Stress and Deflection with Earlier Studies [25][26]

Study	Blade Mass(Kg)	Length of Blade (m)	Tip Deflection (m)	Maximum Stress (MPa)
Present Study	7595.12	35	2.34	181
Zhu, J[25]		38		90
Cai,X[26]	6543.6	37	4.65	

Table 5.7: Comparison of Fundamental Frequency with Earlier Studies [25][26][27]

Study	Blade Mass (Kg)	Length of Blade (m)	First Natural Frequency (Hz)	Percentage Deviation (%)
Present Study	7595.12	35	1.408	0
Zhu, J [25]		38	1.01	39.41
Cai, X [26]	6543.6	37	1.009	39.54
Sandia [27]	4108	30	1.61	12.55

Stress and deflection seems to be off by a factor of 2, and fundamental frequency is off by values shown in table above. This can be attributed to a couple of factors.

1. The length of the blade is not the same.
2. The airfoil shape for the blade cross-section is not specified in the reference study.
3. The longitudinal profile is not specified in the study.
4. Material properties are not completely specified in the reference study. Though the study specifies that it uses all-glass fiber construction it doesn't specify the material properties. So for our analysis, typical values of composite glass fiber were used. Refer Table 3.1 for typical values of glass fiber.
5. The loading in our reference study [25][26] is a series of concentrated loading unlike our present study. So the loading was simulated for validation as close as possible (shown in figures 5.3 and 5.4)
6. The mesh adopted in our present study is a course mesh and that in the reference study [25][26] is very fine mesh having 27,453 elements and 80,687 nodes.

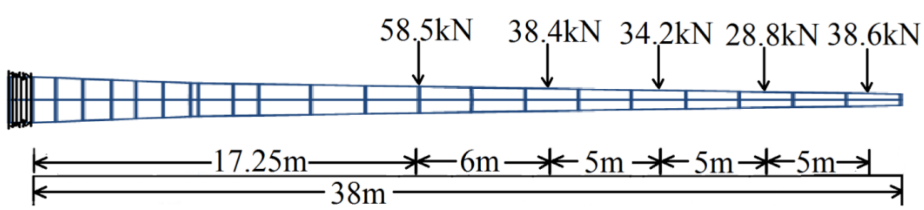

Figure 5.25: Loading Conditions in Zhu, J [25]

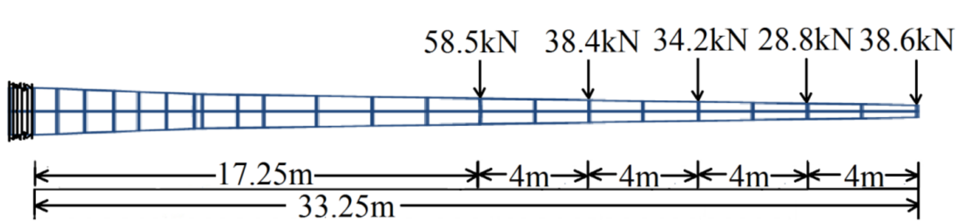

Figure 5.26: Approximated Loading conditions on the present model from Zhu, J [25] Model

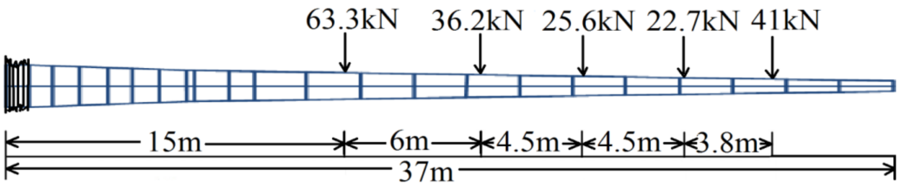

Figure 5.27: Loading conditions in [26]

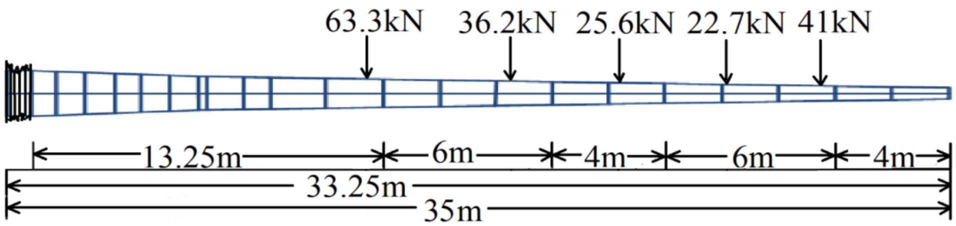

Figure 5.28: Approximated Loading conditions on the present model from [26] Model

CHAPTER 6: DISCUSSIONS

6.1: Static Deflection

From section 5.1.1 and 5.2.1, deflection is seen to be lower for all the retracted blades compared to the conventional blade. In fact the more the blade is retracted, lower the deflection. It is lowest for blade 7 (having retracted length of 21.25m). In chapter 5, an image of the blade above the graph shows specifically the location of the sections along the length of the blade.

Figure 6.1 and 6.2 shows percentage reduction in static deflection when extendable blades are used instead of conventional blades. There is about 16% reduction in deflection in Blade 2 compared to Blade 1, and about 80% reduction in deflection compared to that of Blade 1. In the x-axis, along with the blade name, percentage reduction in length compared to that of blade 1 is also specified.

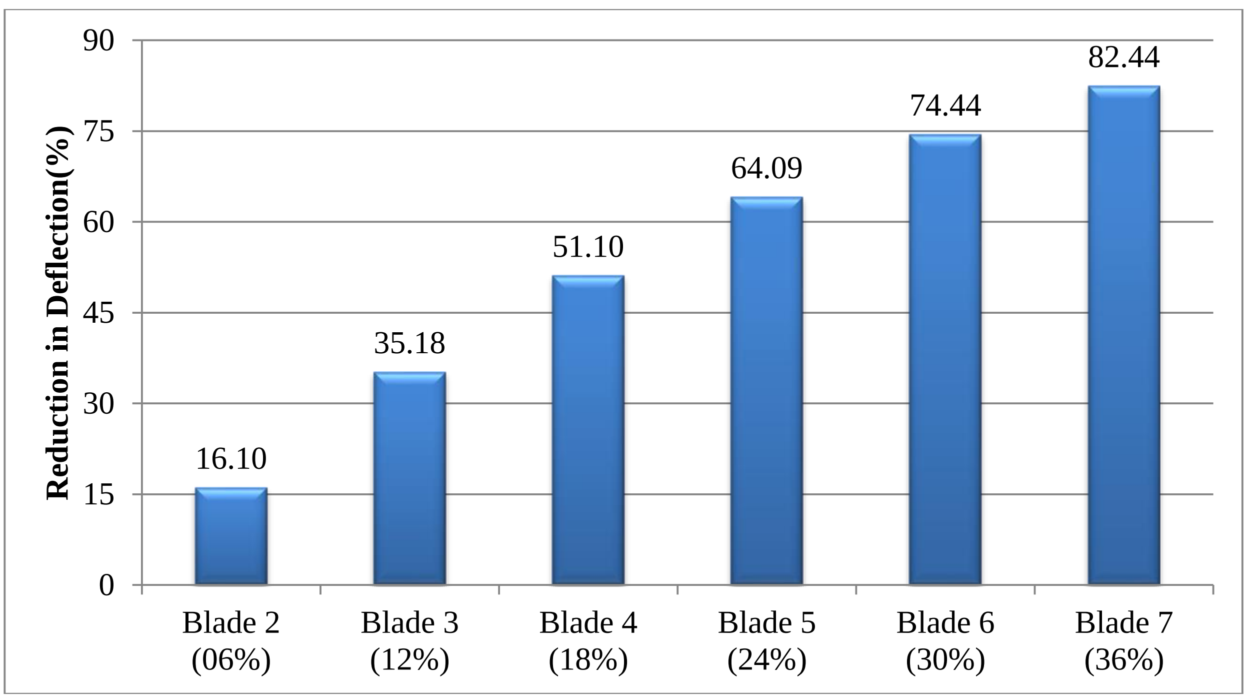

Figure 6.1: Percentage Reduction in Static Deflection (W only)

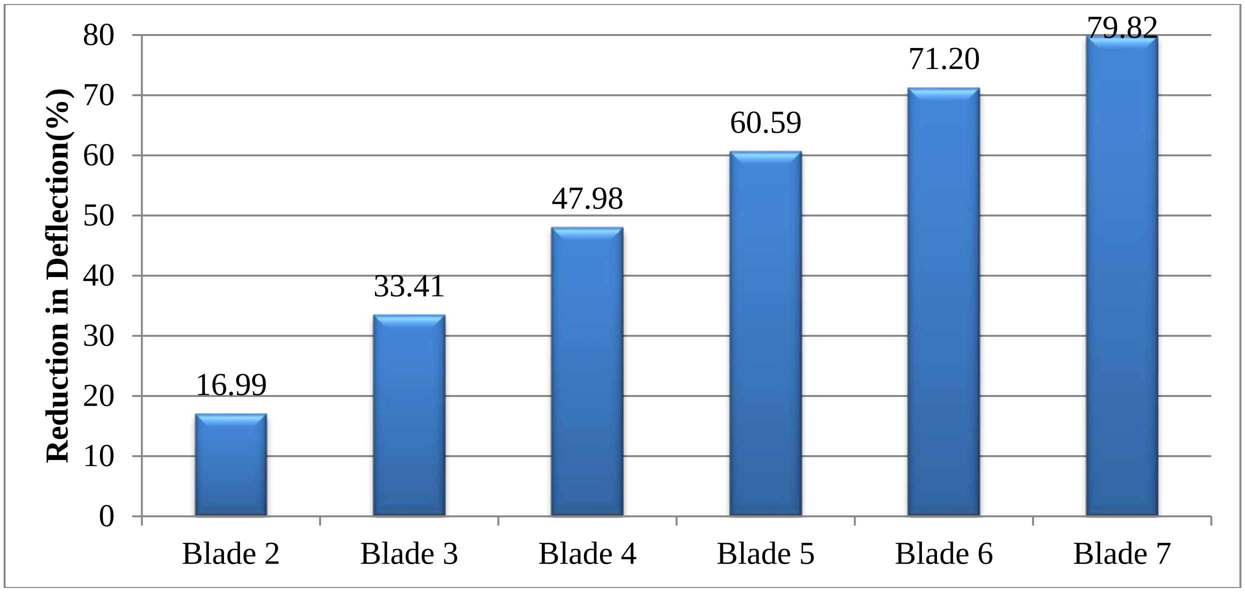

Figure 6.2: Percentage Reduction in Static Deflection

6.2: Stresses

Stresses were computed at the gauss points for all the elements and hence the results are not end of sections but for each elements. As mentioned earlier the stresses peak at the 8th portion (about 7 m from the root of the blade). There is also a minor peak at the 16th portion of the blade (about 20m from the root of the blade).

In our analysis, shell is assumed to have no laminate layer stack up, and behave as a single layer of uniform material. This irregular variation of stresses above can be attributed to that. In addition minor stress peaks also occur, unlike practical stress variation for a cantilever beam. In practical case shell would be lighter and play a minor role in determining stresses and deflection. Hence have a smooth variation of stress throughout the length of the blade.

Figure 6.3 to 6.6 shows percentage reduction in longitudinal and transverse stresses, respectively for retracted blade positions. There is a reduction of about 4-5% in stress, in Blade 2 compared to Blade 1. This may not be a huge margin, but in the Blade 7 there is about 50% reduction of stresses in both longitudinal and transverse stresses.

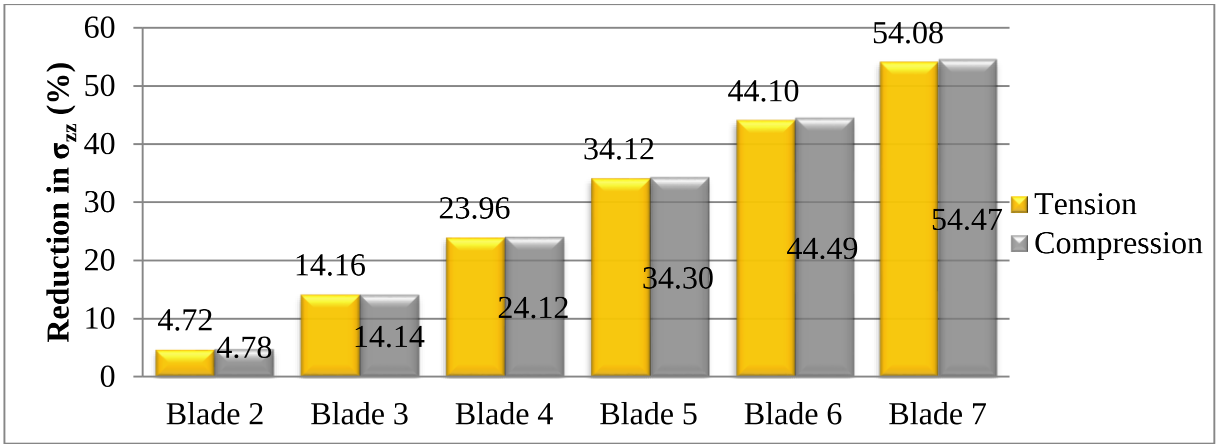

Figure 6.3: Percentage reduction in Longitudinal Stress (W only)

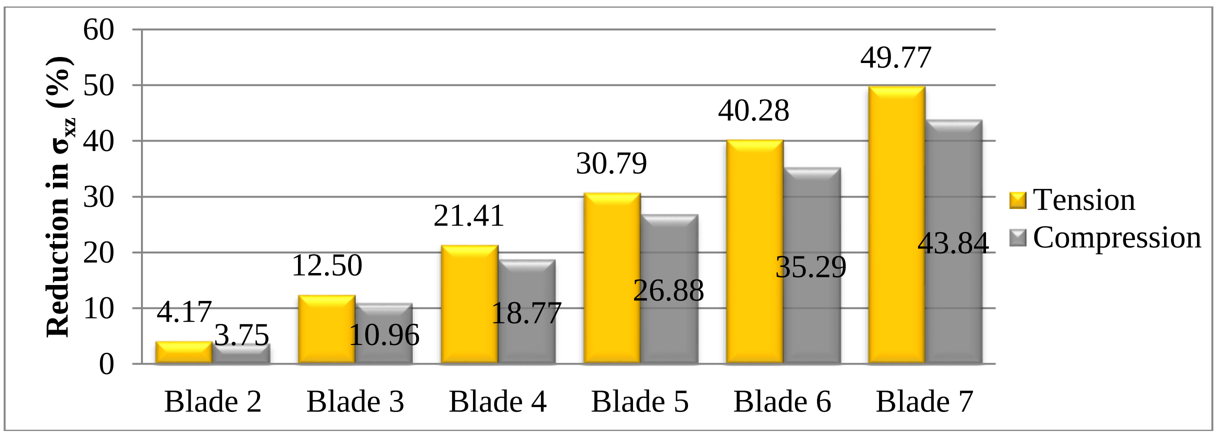

Figure 6.4: Percentage Reduction in Transverse Stress (W only)

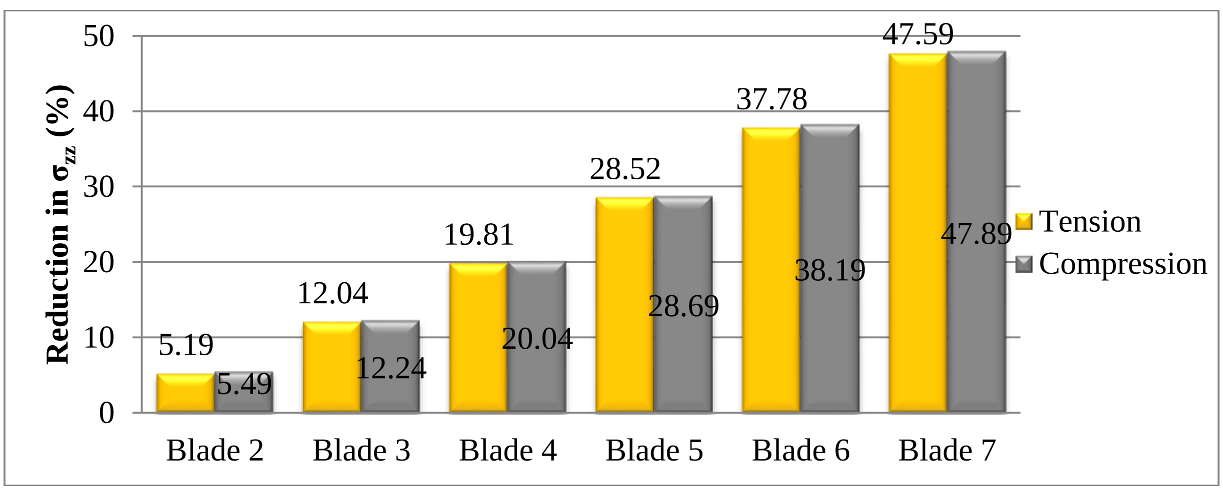

Figure 6.5: Percentage Reduction in Longitudinal Stress (W+D)

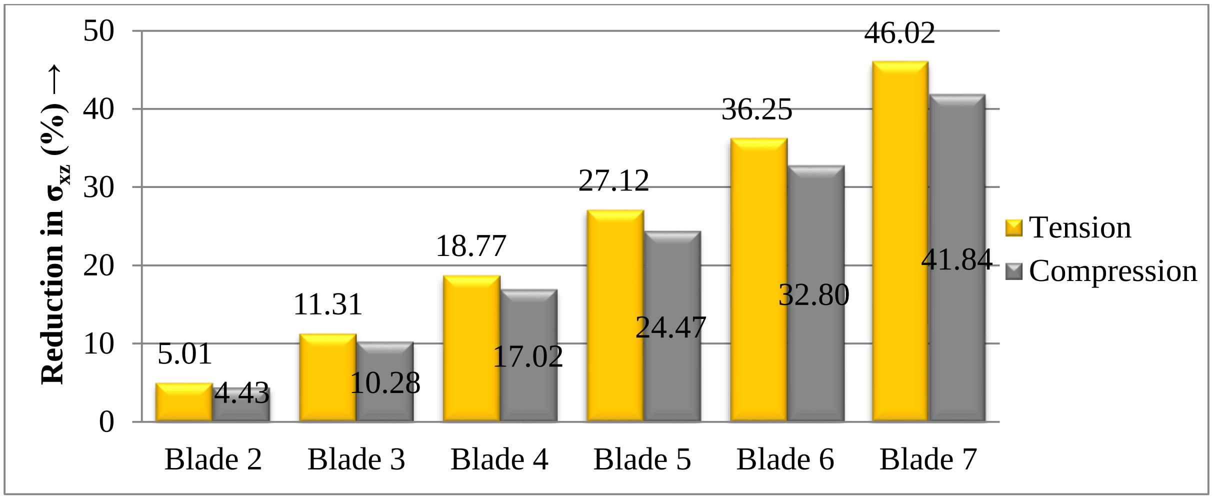

Figure 6.6: Percentage Reduction in Transverse Stress (W+D)

6.3: Fundamental Frequency of Vibration

As expected, the frequency of vibration increases due to the retraction of the blade (Table 5.4). Firstly, vibrational frequency is inversely proportional to blade length, hence it is lower for the retracted blades. Secondly, since the mass remains the same for all the blades, it is distributed over a short length for the retracted blades.

And comparing the modes of vibration for all the blades, they are the same for the first four modes. Mode 1 and mode 3 are Flapwise mode of vibration and, mode 2 and mode 4 are edgewise mode of vibration. But Mode 5 and 6 are not the same for all the blades as clear from Table 5.5. Figure 5.23 and 5.24, also points to the same fact.

Table 5.5 shows the increase in frequency of vibration for all the modes, in the retracted blades compared to Blade 1.

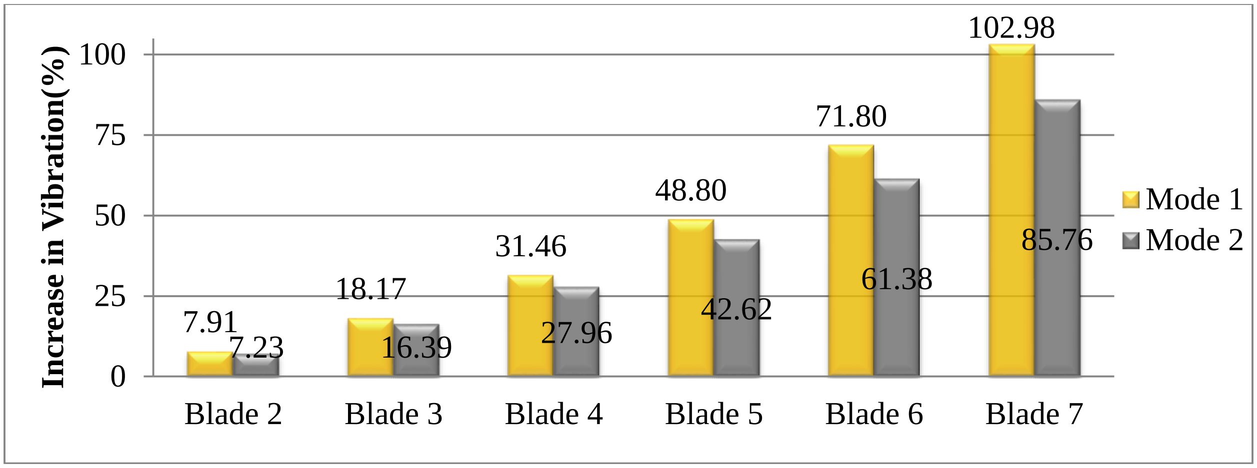

Figure 6.7: Percentage increase in Vibrational Frequency compared to Blade 1 (Mode 1 and 2)

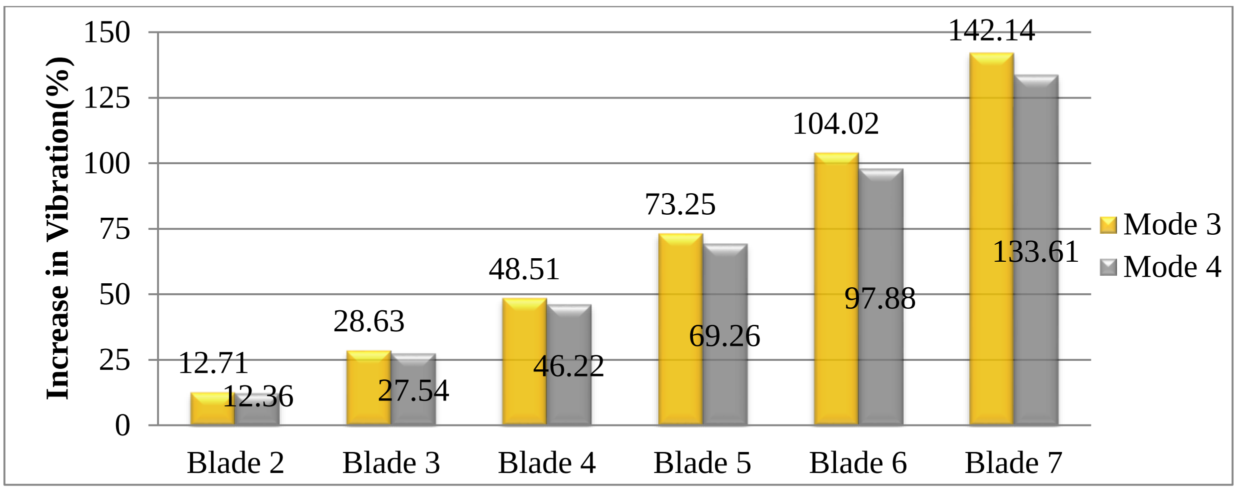

Figure 6.8: Percentage increase in Vibrational Frequency compared to Blade 1 (Mode 3 and 4)

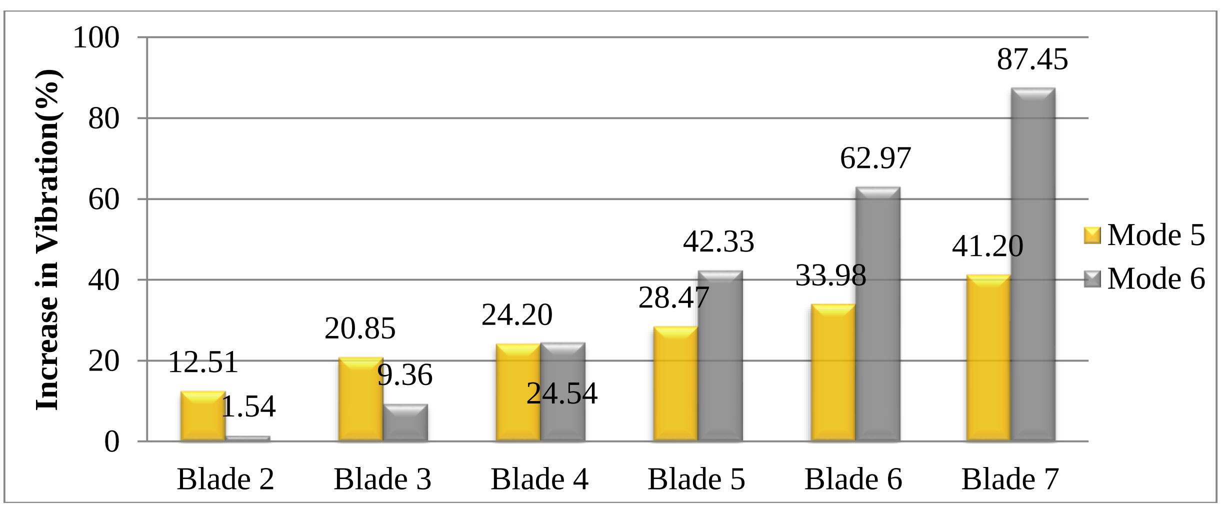

Figure 6.9: Percentage increase in Vibrational Frequency compared to Blade 1 (Mode 5 and 6)

CHAPTER 7: CONCLUSION

So the conclusions can be summed up as below:

7. The deflection of the blade decreases by percent, roughly about 2.5 times for every percent reduction in length of blade. Hence making the blade extendable causes the blade to be stiffer.
8. Percentage reduction in stress is roughly the same amount as the percentage reduction in length of the blade. So making blade extendable causes the blade to be functional over a larger spectrum of wind loading, since it can take up more stress.
9. There is rapid increase in fundamental frequency for every percent reduction in length. Increase in frequency is less for the first few blades and high for the later few.
10. Reduction in deflection and stress favors the use of extendable blades, but at the same time the increase in the fundamental frequencies, means there is limits to which you can make the blade extendable. By using blade 7, the fundamental frequencies increase by about 100%, i.e. for reduction of length of 36%, the fundamental frequencies double. So the amount by which the blade is to be made retractable is determined by the site conditions of wind loading, climate and provision for transportation.

REFERENCES

1. Subbaiah. V. Pasupulati, Jack Wallace, Mark Dawson (2005). Variable Length Blades Wind Turbine, *Power Engineering Society, Institute of Electrical And Electronics Engineers*, June 2005.
2. Dayton A. Griffin (2002). Blade System Design Studies Volume I: Composite Technologies for Large Wind Turbine Blades, *SAND2002-1879. Albuquerque, NM: Sandia National Laboratories.*
3. History of Wind Energy, from Iowa Energy Centre http://www.iowaenergycenter.org/wind-energy-manual/history-of-wind-energy/. Revisited in 20 January 2014
4. Timeline: History of Wind Power, from The Guardian http://www.theguardian.com/environment/2008/oct/17/wind-power-renewable-energy. Revisited in 27 January 2014
5. Carl Sulzberger (2009). A bold effort in Vermont, *Power And Energy Magazine*, *Institute of Electrical And Electronics Engineers,Vol.7, Issue 6*, Pages 100-110
6. The Wind Energy Pioneers: The Gedser wind Turbine, Updated 23 July 2003, *Danish Wind Energy Association,* *http://www.motiva.fi/myllarin_tuulivoima/windpower%20web/en/pictures/juul.htm* Retrieved 3 February 2014.
7. Seanergy 2020: Final Project summary, May 2012.
8. Poul Sørensen, Nicolaos Antonio Cutululis, Antonio Vigueras-Rodríguez, Henrik Madsen, Pierre Pinson, Leo E. Jensen, Jesper Hjerrild and Martin

Donovan(2008).Modelling of power fluctuations from large offshore wind farms, *Wind Energy*, vol.11,Issue 1,Pages 29-43, January 2008

9. 10 Biggest Turbines in the world, from Wind Power Monthly, http://www.windpowermonthly.com/10-biggest-turbines . Revisited in 27 January 2014
10. Gary L. Johnson, 1985. *Wind Energy Systems*, Illustrated, Prentice Hall PTR, London,1985 (Digitalized in July 2008)
11. V. A. Riziotis, S. G. Voutsinas, E. S. Politis and P. K Chaviaropoulos (2004). Aeroelastic stability of wind turbines: the problem, the methods and the issues, *Wind Energy*, Vol.7,Issue 4, November 2004
12. Patrick. J. Moriarty, William E. Holley, Sandy Butterfield (2002). Effect Of Turbulence Variation On Extreme Loads Prediction For Wind Turbines, *American Society of Mechanical Engineers*, Vol. 124, Issue 4, Pages 387-395, November 2002.
13. Freight Management and Operations, Federal Highway Administration, U.S. Department of Transportation, from, http://ops.fhwa.dot.gov/Freight/publications/size_regs_final_rpt/index.htm . Revisited in 3 November 2014.
14. R.N. Sharma and U. Madawala (2007). The Concept of a Smart Wind Turbine System, Renewable Energy, Vol.39, Issue 1, Pages 403-410,March 2012.
15. Mustahib Imraan, Rajnish.N.Sharma and Richard.G.J. Flay (2009). Telescopic wind Turbine to Capture Energy at Low Wind Speed, *The American Society of Mechanical Engineers*, January 2009.

16. Mustahib Imraan, Rajnish. N. Sharma and Richard. G. J. Flay (2011). Wind Tunnel Testing of a Telescopic Blade Wind Turbine, *The American Society of Mechanical Engineers*, January 2011.

17. Tartibu, L.K., Kilfoil, M. And Van Der Merwe, A.J (2012). Vibration Analysis Of A Variable Length Blade Wind Turbine, *International Journal of Advances in Engineering & Technology*, Vol 4, Issue 1, Pages 630-639, July 2012.

18. Timothy J McCoy and Dayton A Griffin (2006). Active control of rotor aerodynamics and geometry: Status, methods, and preliminary results, *American Institute of Aeronautics and Astronautics Inc.*, In 44th AIAA/ASME.

19. Timothy J McCoy and Dayton A Griffin (2008). Control of rotor geometry and aerodynamics: Retractable Blades and Advanced Concepts, *Multi-Science Publishing Co. Ltd*, Vol. 32, Issue 1, Pages 13-26, January 2008.

20. Hodges, D. H.; and Dowell, E. H (1974). Nonlinear Equations of Motion for the Elastic Bending and Torsion of Twisted Non-uniform Rotor Blades, *NASA TN D-7818*

21. J.W. Larsen, S.R.K. Nielsen (2006). Nonlinear parametric instability of wind turbine wings, *Journal of Sound and Vibration*, Vol 299, Issue 1-2, Pages 64-82.

22. Beth Stackpole, Contributing Editor, Design Software & Hardware (January 2011) Sandia Sizes up Wind Turbine Blade Design. Retrieved from http://www.designnews.com/document.asp?doc_id=230008 , Revisited in January 2014.

23. Mechanical Properties of Carbon Fibre Composite Materials, Fibre / Epoxy resin (120°C Cure), http://www.performancecomposites.com/about-composites-technical-info/122-designing-with-fiberglass.html , Performance Composites Ltd., Revisited in February 2014.

24. J. Jonkman, S. Butterfield, W. Musial, and G. Scott (February 2009). Definition of a 5MW Reference Wind Turbine for Offshore System Development, *National Renewable Energy Institute, NREL/TP-500-38060*. Revisited in June 2014.

25. Zhu J, Xin C, Pan P, Rongrong G (January 2012). Static And Dynamic Characteristics Study Of Wind Turbine Blade, *Advanced Materials Research 2012; 433-440: 438–44*. Revisisted in January 2015.

26. Xin Cai, Jie Zhu, Pan Pan, and Rongrong Gu (November2012). Structural Optimization Design of Horizontal-Axis Wind Turbine Blades Using a Particle Swarm Optimization Algorithm and Finite Element Method. *Energies, 5(11):4683–4696*,Revisited in January 2015

27. TPI Composites, (May 2003). Cost Study for Large Wind Turbine Blades: WindPACT Blade System Design Studies, *SAND2003-1428. Albuquerque, NM: Sandia National Laboratories.*

APPENDIX A: ADDITIONAL MODELLING DETAILS

Section 1 and 2:

The blade at the root has constant cross section for 0.7 meters. The section is as shown below. In theory the blade at the root is round and the round section is approximately modelled into an octagonal shape as shown in figure.7.1.

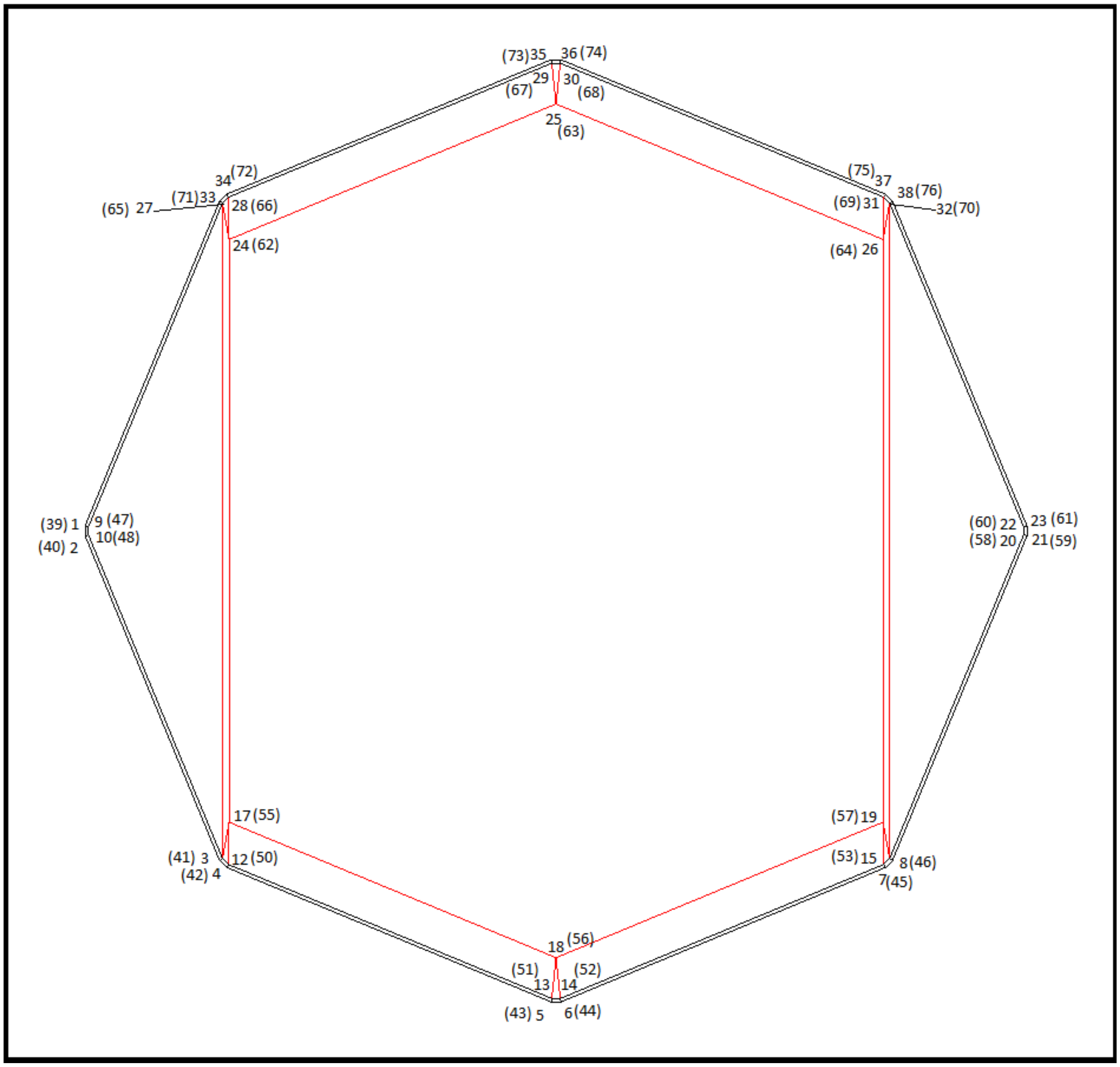

Figure A.1 : Nodal and Element Details of Section 1 and 2

The section has 38 nodes all together. The black lines essentially sketch the shell and the red lines mark the box spar. There are two sections of the same shape at 0.7m spacing having 38 nodes each. In the image above the node numbering in the bracket are that of the second section. The node numbering in the brackets are that of section 2 and the other is that of section 1.

Section 3:

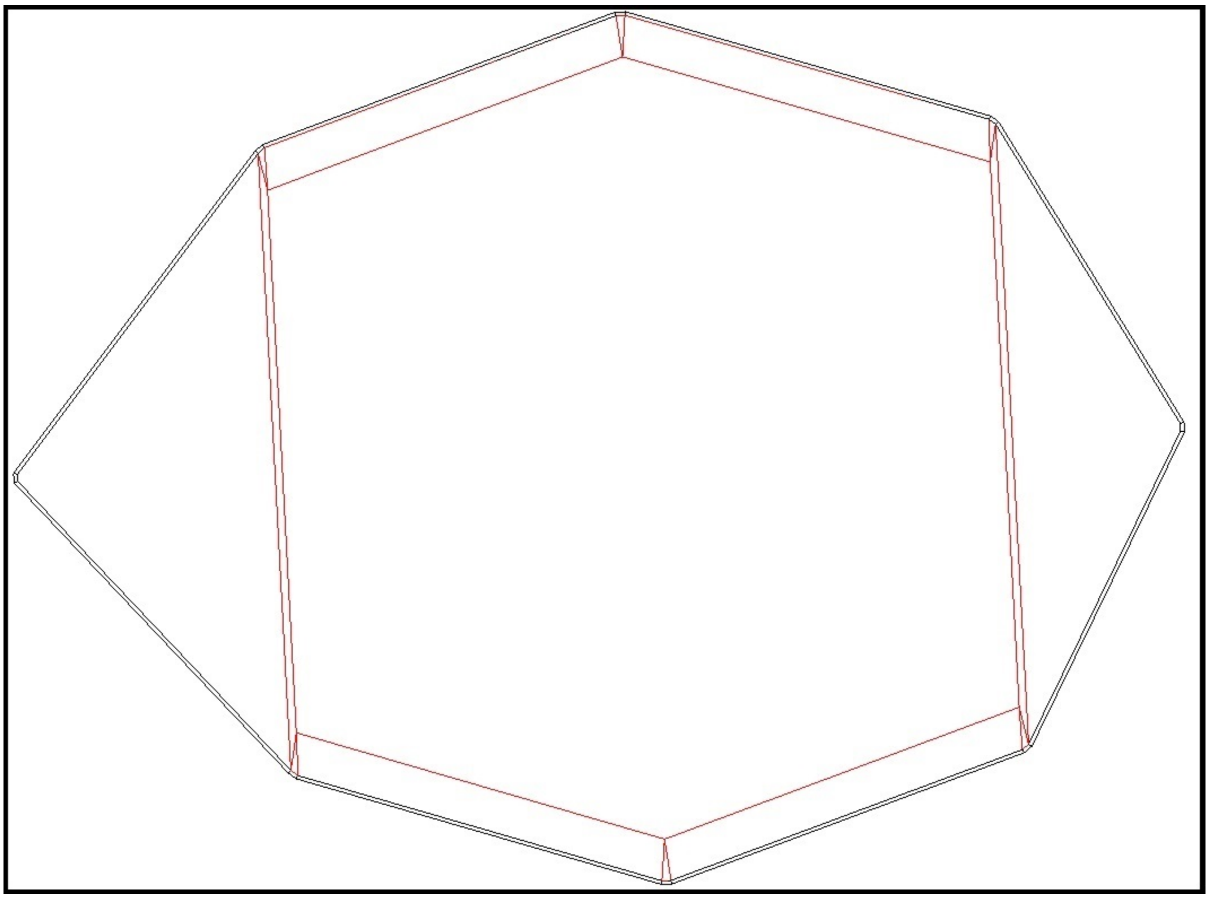

Figure A.2: Element details of Section 3

From the 9th section to the 23rd all of them have the s818 airfoil shape. Sections in between the 2nd to the 9th are transition sections. The transition is from the octagonal shape of the 2nd section to the airfoil shape of the 9th section. The 3rd section is as shown above. It has lost the round shape and is not airfoil shape. It has 38 nodes just like the 2nd section hence they can be easily interconnected.

Other Sections:

Then the sections get more airfoil shape as we move from the 3rd section to the 8th section. These sections are as shown below from figures 7.3 to 7.7.

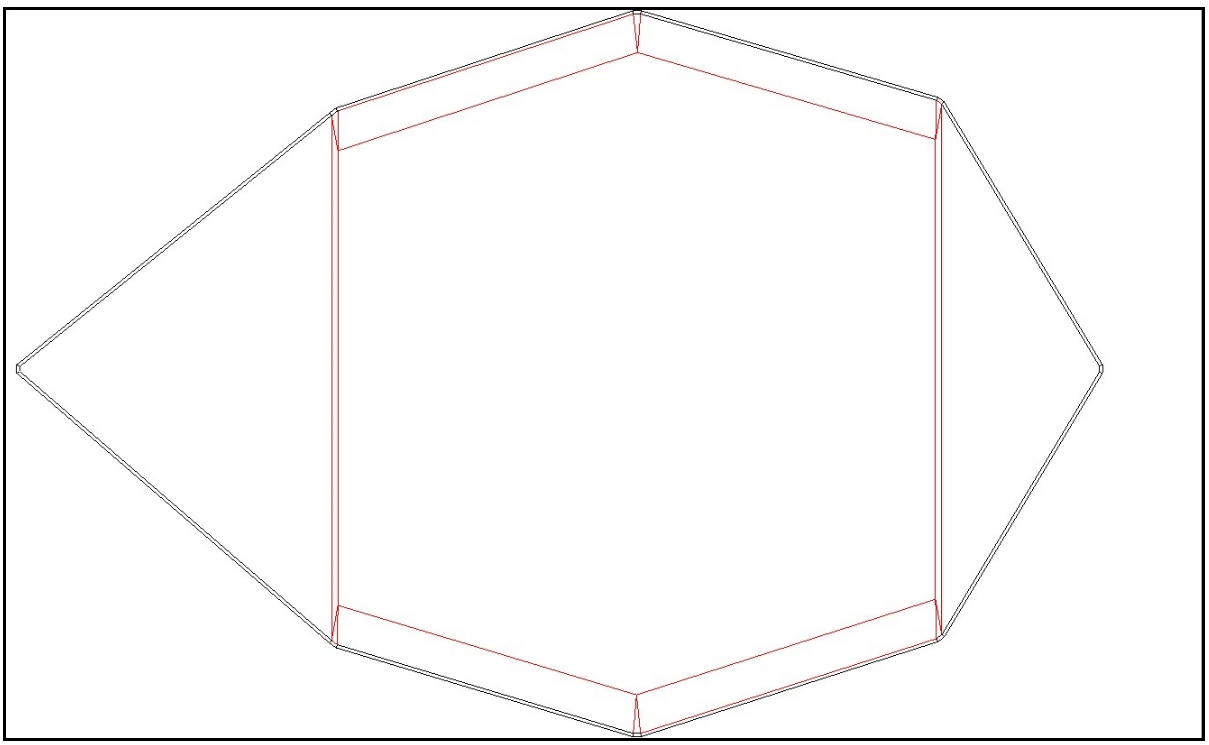

Figure A.3: Element details of Section 4

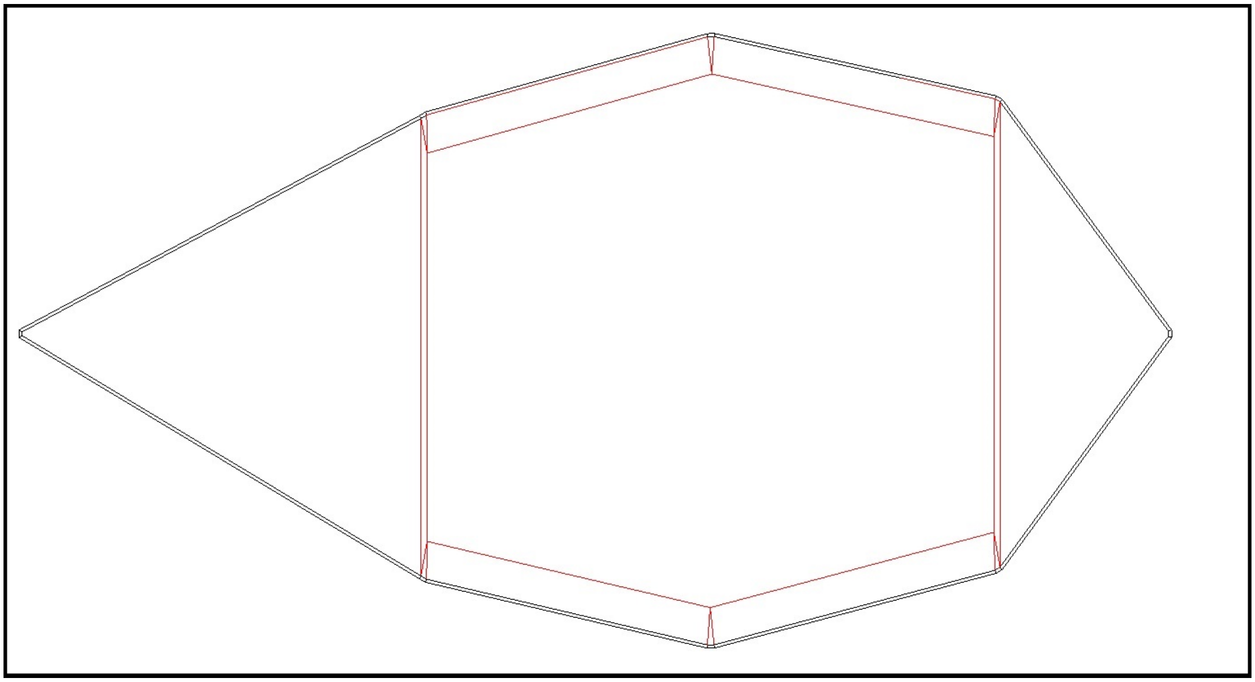

Figure A.4: Element details of Section 5

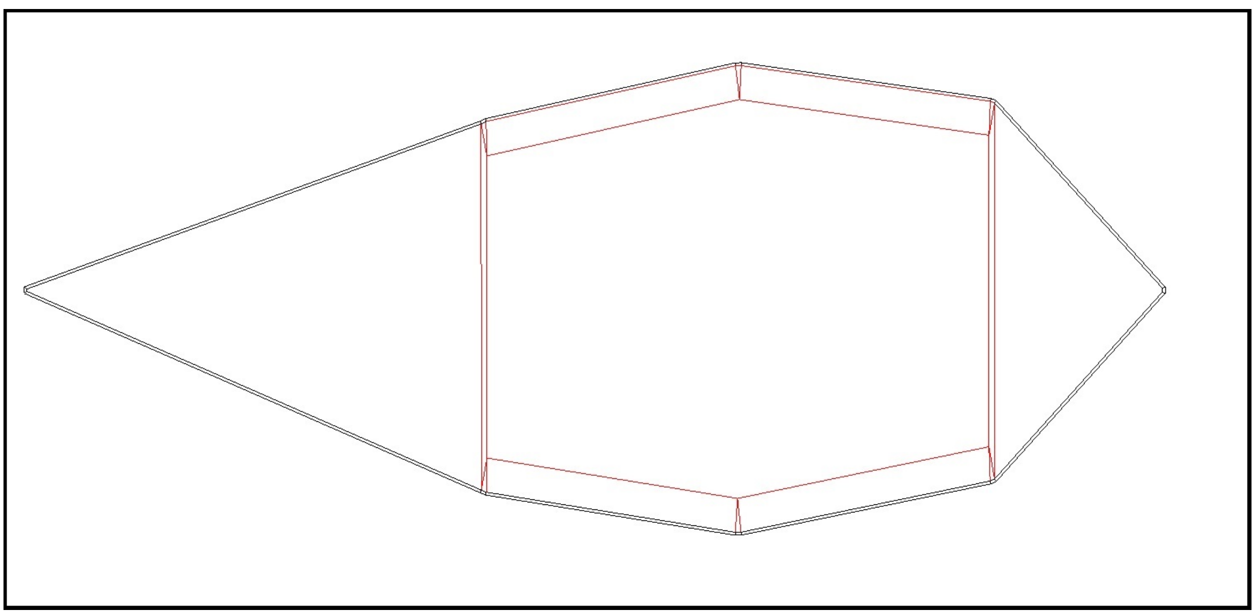

Figure A.5: Element details of Section 6

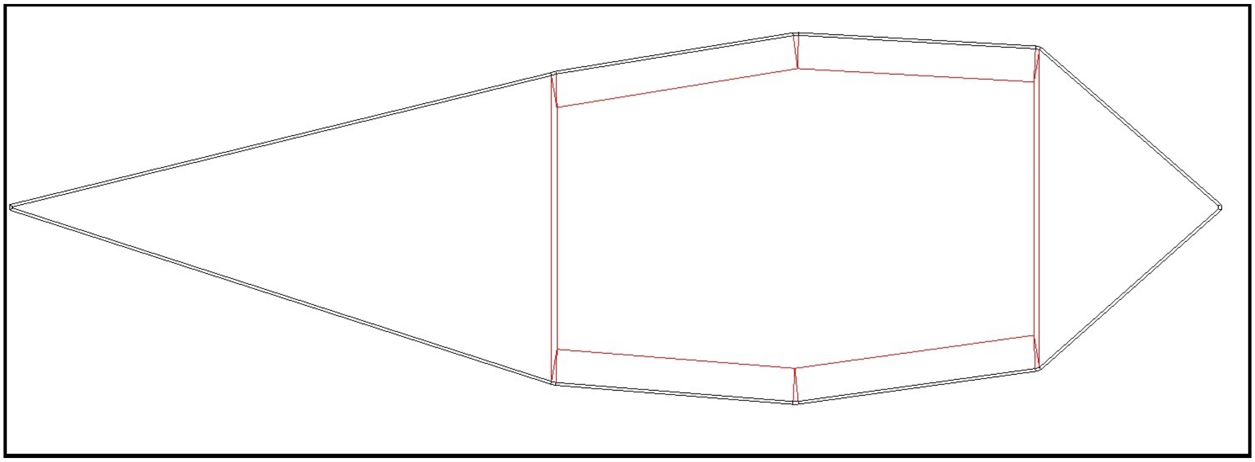

Figure A.6: Element details of Section 7

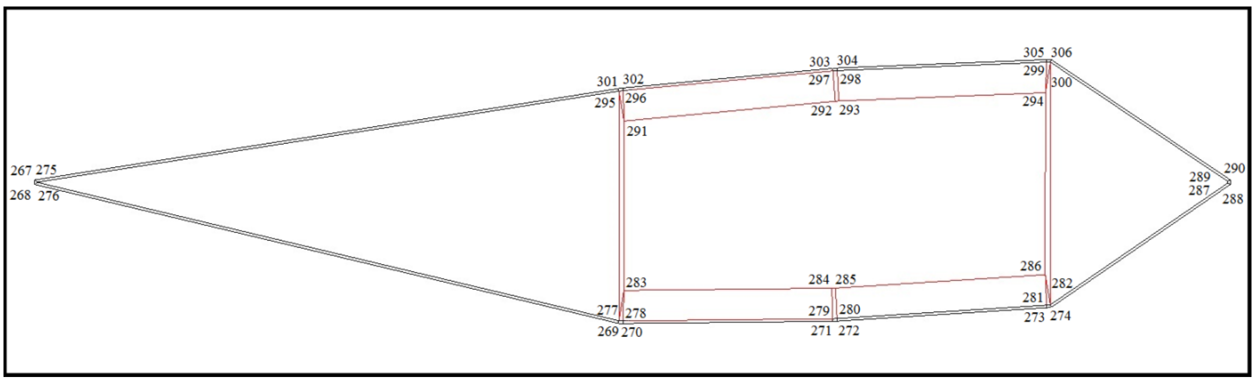

Figure A.7: Element details of Section 8

The 8th section is almost airfoil shape and has 40 nodes and required use of 7-noded elements to join it to the 7th section. During the analysis the 7-noded element is treated as an 8-noded element with the beginning node repeating itself at the end.

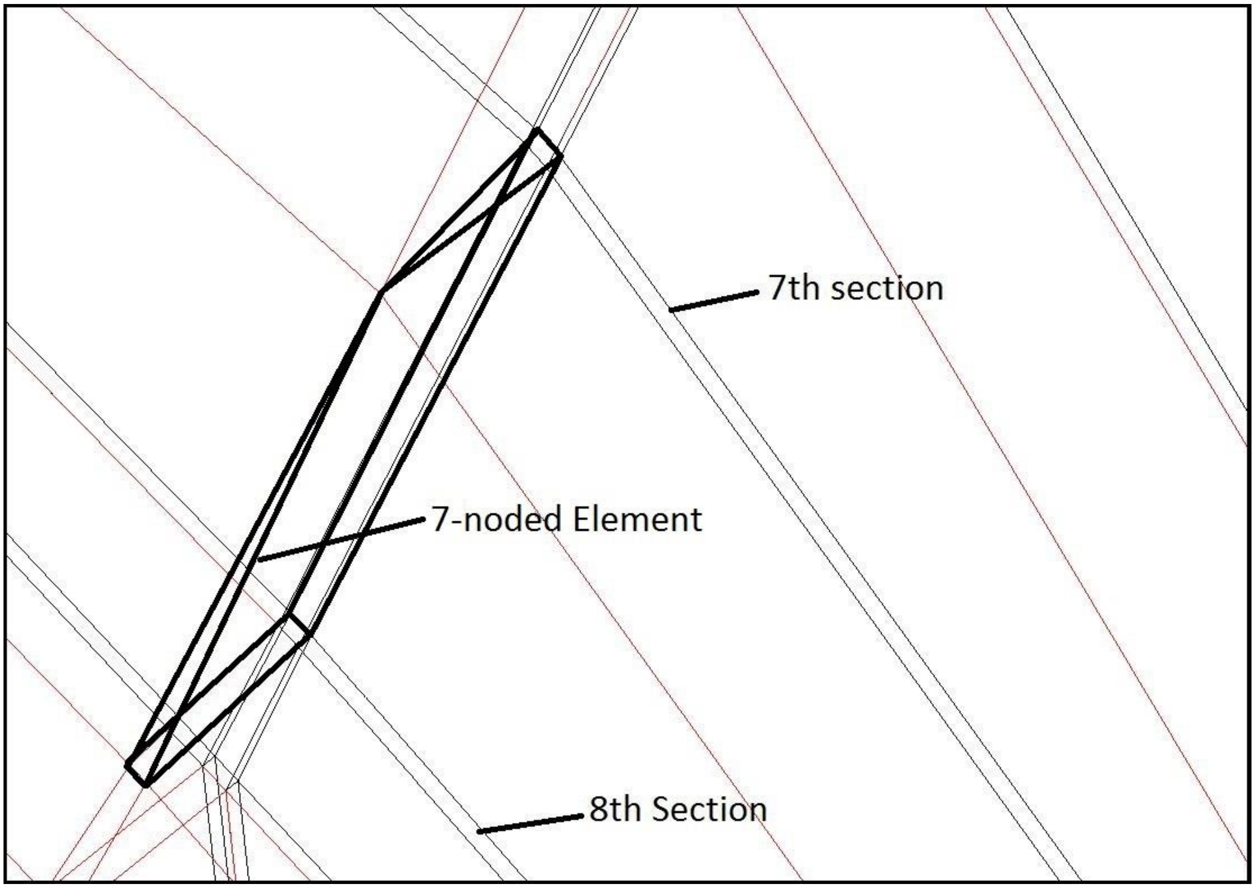

Figure A.8: 7-noded element

The 9th section is the largest section on the blade and is as shown in Figure 3.7 in chapter 3. It has a chord length of 2.84m from the outer ends of the shell. It reduces in chord length as it moves from 9th section to the 23rd section. The 23rd section has a chord length of 0.925m from the outer ends of the shell.

And Figure 7.9 shows a complete isometric view of the entire modelled blade. Specifically this depicts the 33.25 m long Blade 1without any retraction.

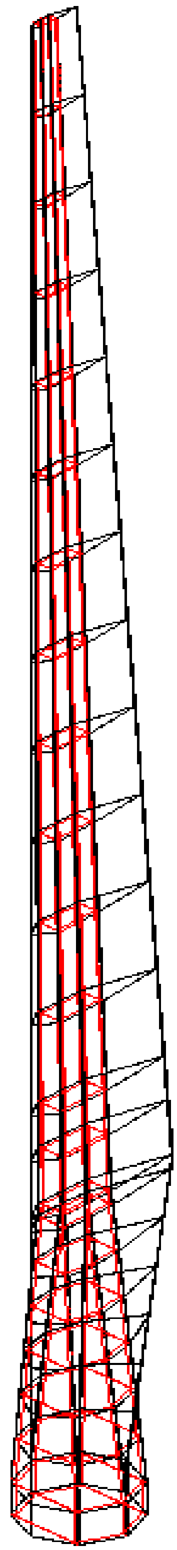

Figure A.9:Isometric view of the Blade

APPENDIX B: ADDITIONAL DETAILS FOR RESULT

Load Case 1(Wind Load Only)

1. Static Deflection:

The calculated deflections were condensed to the below tabulated data for plotting graph.

Table B.1: Static Deflection Data for each Blade (Wind Load only)

Section	Blade 1	Blade 2	Blade 3	Blade 4	Blade 5	Blade 6	Blade 7
1	0.0000	0.0000	0.0000	0.0000	0.0000	0.0000	0.0000
2	0.0000	0.0000	0.0000	0.0000	0.0000	0.0000	0.0000
3	0.0000	0.0000	0.0000	0.0000	0.0000	0.0000	0.0000
4	0.0000	0.0000	0.0000	0.0000	0.0000	0.0000	0.0000
5	0.0001	0.0001	0.0001	0.0001	0.0001	0.0001	0.0001
6	0.0001	0.0001	0.0001	0.0001	0.0001	0.0001	0.0001
7	0.0002	0.0002	0.0002	0.0002	0.0002	0.0002	0.0001
8	0.0003	0.0003	0.0003	0.0003	0.0003	0.0002	0.0002
9	0.0004	0.0004	0.0003	0.0003	0.0003	0.0003	0.0002
10	0.0008	0.0008	0.0007	0.0007	0.0006	0.0005	0.0005
11	0.0013	0.0012	0.0011	0.0010	0.0009	0.0008	0.0007
12	0.0024	0.0023	0.0021	0.0019	0.0017	0.0015	0.0012
13	0.0037	0.0036	0.0032	0.0029	0.0025	0.0022	0.0018
14	0.0053	0.0050	0.0045	0.0040	0.0035	0.0030	0.0025
15	0.0070	0.0066	0.0060	0.0052	0.0045	0.0038	0.0031
16	0.0089	0.0084	0.0075	0.0066	0.0056	0.0047	0.0038
17	0.0109	0.0103	0.0091	0.0079	0.0067	0.0056	0.0044
18	0.0131	0.0124	0.0109	0.0094	0.0079	0.0065	
19	0.0155	0.0145	0.0127	0.0109	0.0091		
20	0.0179	0.0168	0.0146	0.0124			
21	0.0204	0.0190	0.0164				
22	0.0229	0.0213					
23	0.0254						

And the readings in red are the tip deflections which are the maximum deflections occurring in the corresponding blade.

2. Longitudinal Stresses:

The details below were used to plot the graphs depicting variation of stress over the length of the blade.

Stress in Tension:

Table B.2: Data for Longitudinal Stress in tension (W only)

Portion	Location*	Blade 1	Blade 2	Blade 3	Blade 4	Blade 5	Blade 6	Blade 7
1	0.35	1.25	1.21	1.12	1.04	0.945	0.85	0.753
2	1.2	1.28	1.24	1.14	1.05	0.947	0.843	0.739
3	2.2	1.48	1.43	1.32	1.2	1.08	0.959	0.834
4	3.2	1.71	1.65	1.52	1.38	1.23	1.08	0.933
5	4.2	2.01	1.93	1.76	1.59	1.41	1.23	1.05
6	5.2	2.48	2.36	2.13	1.88	1.66	1.44	1.22
7	6.2	3.57	3.39	3.05	2.68	2.32	1.95	1.59
8	6.85	5	4.76	4.29	3.8	3.3	2.79	2.3
9	7.625	4.06	3.85	3.45	3.03	2.6	2.17	1.76
10	8.75	3.31	3.14	2.79	2.43	2.07	1.71	1.37
11	10.25	2.54	2.39	2.11	1.82	1.53	1.24	0.971
12	12.25	2.11	1.97	1.71	1.44	1.18	0.924	0.688
13	14.25	1.82	1.68	1.43	1.18	0.932	0.699	0.489
14	16.25	1.57	1.44	1.19	0.943	0.709	0.495	0.311
15	18.25	1.26	1.13	0.895	0.667	0.458	0.279	0.139
16	20.25	1.24	1.1	0.835	0.589	0.374	0.198	0.078
17	22.25	0.956	0.821	0.582	0.369	0.198	0.062	
18	24.25	0.722	0.593	0.376	0.201	0.065		
19	26.25	0.505	0.387	0.206	0.065			
20	28.25	0.304	0.206	0.065				
21	30.25	0.155	0.072					
22	32.25	0.044						

*It is the distance from the root of the blade to center of corresponding portion in meters.

Stress in Compression:

Table B.3: Data for Longitudinal Stress in compression (W only)

Portion	Location*	Blade 1	Blade 2	Blade 3	Blade 4	Blade 5	Blade 6	Blade 7
1	0.35	1.25	1.2	1.12	1.03	0.939	0.843	0.746
2	1.2	1.25	1.21	1.12	1.03	0.928	0.828	0.726
3	2.2	1.38	1.33	1.22	1.11	1	0.887	0.772
4	3.2	1.57	1.51	1.39	1.26	1.12	0.987	0.851
5	4.2	1.81	1.74	1.59	1.43	1.27	1.11	0.948
6	5.2	2.23	2.13	1.93	1.71	1.49	1.28	1.07
7	6.2	3.2	3.04	2.74	2.42	2.1	1.77	1.45
8	6.85	4.5	4.28	3.85	3.41	2.95	2.5	2.05
9	7.625	3.57	3.39	3.04	2.67	2.29	1.92	1.56
10	8.75	3.31	3.13	2.78	2.42	2.05	1.69	1.34
11	10.25	2.45	2.31	2.03	1.75	1.46	1.18	0.915
12	12.25	2.06	1.93	1.67	1.4	1.14	0.882	0.647
13	14.25	1.96	1.81	1.52	1.23	0.955	0.696	0.465
14	16.25	1.33	1.22	1.01	0.8	0.603	0.424	0.269
15	18.25	1.1	0.987	0.78	0.581	0.398	0.246	0.126
16	20.25	1.39	1.23	0.942	0.669	0.428	0.23	0.092
17	22.25	0.885	0.754	0.523	0.327	0.173	0.056	
18	24.25	0.677	0.55	0.34	0.174	0.056		
19	26.25	0.465	0.351	0.18	0.057			
20	28.25	0.276	0.182	0.059				
21	30.25	0.132	0.060					
22	32.25	0.039						

*It is the distance from the root of the blade to center of corresponding portion in meters.

3. Transverse Stress

Stress in Tension:

Table B.4: Data for Transverse Stress in tension (W only)

Portion	Location*	Blade 1	Blade 2	Blade 3	Blade 4	Blade 5	Blade 6	Blade 7
1	0.35	0.0354	0.035	0.033	0.031	0.029	0.027	0.025
2	1.2	0.0407	0.039	0.036	0.032	0.029	0.026	0.023
3	2.2	0.0705	0.067	0.061	0.054	0.047	0.042	0.036
4	3.2	0.0902	0.086	0.078	0.069	0.060	0.051	0.043
5	4.2	0.112	0.107	0.096	0.085	0.074	0.062	0.051
6	5.2	0.141	0.134	0.120	0.106	0.092	0.078	0.063
7	6.2	0.192	0.183	0.165	0.146	0.126	0.110	0.088
8	6.85	0.317	0.303	0.273	0.243	0.211	0.180	0.149
9	7.625	0.472	0.457	0.426	0.393	0.357	0.320	0.281
10	8.75	0.543	0.523	0.484	0.442	0.398	0.352	0.304
11	10.25	0.634	0.608	0.555	0.499	0.441	0.381	0.32
12	12.25	0.445	0.427	0.39	0.350	0.308	0.265	0.221
13	14.25	0.369	0.352	0.318	0.282	0.244	0.205	0.165
14	16.25	0.307	0.291	0.257	0.222	0.185	0.148	0.112
15	18.25	0.269	0.251	0.214	0.177	0.139	0.102	0.068
16	20.25	0.272	0.251	0.209	0.166	0.123	0.082	0.047
17	22.25	0.263	0.239	0.193	0.145	0.099	0.058	
18	24.25	0.226	0.201	0.151	0.103	0.060		
19	26.25	0.182	0.154	0.105	0.060			
20	28.25	0.135	0.108	0.061				
21	30.25	0.089	0.064					
22	32.25	0.044						

*It is the distance from the root of the blade to center of corresponding portion

Stress in Compression:

Table B.5: Data for Transverse Stress in compression (W only)

Portion	location	Blade 1	Blade 2	Blade 3	Blade 4	Blade 5	Blade 6	Blade 7
1	0.35	0.0085	0.0076	0.0059	0.00585	0.0067	0.0068	0.0072
2	1.2	0.0312	0.029	0.0247	0.0202	0.0158	0.0114	0.0074
3	2.2	0.0538	0.051	0.0452	0.0393	0.0332	0.0271	0.0211
4	3.2	0.0744	0.0706	0.063	0.0551	0.047	0.039	0.0311
5	4.2	0.103	0.098	0.0876	0.0768	0.0657	0.0547	0.0439
6	5.2	0.15	0.142	0.127	0.111	0.0952	0.0792	0.0637
7	6.2	0.249	0.236	0.212	0.186	0.16	0.133	0.108
8	6.85	0.635	0.612	0.567	0.519	0.467	0.414	0.36
9	7.625	0.412	0.402	0.38	0.357	0.33	0.301	0.27
10	8.75	0.653	0.629	0.579	0.526	0.47	0.412	0.352
11	10.25	0.493	0.476	0.441	0.402	0.361	0.317	0.271
12	12.25	0.412	0.396	0.364	0.328	0.29	0.25	0.208
13	14.25	0.331	0.315	0.283	0.249	0.214	0.177	0.139
14	16.25	0.264	0.248	0.216	0.182	0.148	0.113	0.0952
15	18.25	0.277	0.258	0.221	0.182	0.139	0.0947	0.0684
16	20.25	0.308	0.285	0.239	0.188	0.133	0.0961	0.0723
17	22.25	0.286	0.26	0.206	0.148	0.107	0.0925	
18	24.25	0.242	0.213	0.153	0.109	0.0951		
19	26.25	0.197	0.162	0.113	0.0962			
20	28.25	0.141	0.117	0.0955				
21	30.25	0.094	0.0996					
22	32.25	0.0725						

*It is the distance from the root of the blade to center of corresponding portion

<u>Load Case 2 (Dead Load + Wind Load)</u>

1. Static Deflection

The results for static deflection were condensed into the table below for plotting the graphs.

Table B.6: Static Deflection Data for each Blade (Dead Load + Wind Load)

Section	Blade 1	Blade 2	Blade 3	Blade 4	Blade 5	Blade 6	Blade 7
1	0.0000	0.0000	0.0000	0.0000	0.0000	0.0000	0.0000
2	0.0000	0.0000	0.0000	0.0000	0.0000	0.0000	0.0000
3	0.0001	0.0001	0.0001	0.0001	0.0001	0.0001	0.0001
4	0.0003	0.0003	0.0003	0.0003	0.0003	0.0003	0.0003
5	0.0006	0.0006	0.0006	0.0005	0.0005	0.0005	0.0005
6	0.0010	0.0010	0.0010	0.0009	0.0009	0.0008	0.0008
7	0.0016	0.0016	0.0015	0.0015	0.0014	0.0013	0.0012
8	0.0025	0.0024	0.0023	0.0022	0.0021	0.0019	0.0018
9	0.0030	0.0029	0.0027	0.0026	0.0024	0.0023	0.0021
10	0.0063	0.0060	0.0057	0.0053	0.0049	0.0044	0.0039
11	0.0097	0.0093	0.0087	0.0081	0.0074	0.0066	0.0058
12	0.0184	0.0176	0.0164	0.0151	0.0136	0.0120	0.0103
13	0.0286	0.0272	0.0253	0.0231	0.0207	0.0181	0.0153
14	0.0403	0.0381	0.0353	0.0321	0.0285	0.0247	0.0207
15	0.0533	0.0503	0.0464	0.0419	0.0370	0.0318	0.0264
16	0.0675	0.0635	0.0583	0.0524	0.0459	0.0391	0.0321
17	0.0828	0.0776	0.0708	0.0633	0.0551	0.0465	0.0379
18	0.0990	0.0924	0.0840	0.0746	0.0645	0.0540	
19	0.1159	0.1078	0.0975	0.0861	0.0739		
20	0.1335	0.1236	0.1112	0.0976			
21	0.1514	0.1396	0.1249				
22	0.1695	0.1557					
23	0.1876						

2. Longitudinal Stresses:

The details below were used to plot the graphs depicting variation of stress over the length of the blade.

Stress in Tension:

Table B.7: Data for Longitudinal Stress in tension (W+D)

Portion	Location	Blade 1	Blade 2	Blade 3	Blade 4	Blade 5	Blade 6	Blade 7
1	0.35	11.5	11.2	10.7	10.1	9.47	8.75	7.96
2	1.2	11.5	11	10.5	9.88	9.17	8.38	7.53
3	2.2	12.9	12.4	11.8	11	10.2	9.26	8.25
4	3.2	14.7	14.1	13.3	12.4	11.4	10.2	9.04
5	4.2	16.9	16.1	15.2	14.1	12.8	11.5	10
6	5.2	20.2	19.2	17.8	16.3	14.8	13.1	11.3
7	6.2	28.8	27.3	25.2	22.9	20.3	17.6	14.7
8	6.85	40.3	38.2	35.4	32.3	28.8	25	21.1
9	7.625	32	30.2	27.9	25.2	22.2	19	15.8
10	8.75	25.8	24.2	22.2	19.9	17.4	14.7	12
11	10.25	19.4	18.1	16.4	14.6	12.6	10.5	8.32
12	12.25	15.5	14.3	12.8	11.1	9.33	7.47	5.63
13	14.25	13	11.8	10.2	8.59	6.93	5.26	3.67
14	16.25	10.5	9.39	7.98	6.47	4.93	3.45	2.13
15	18.25	8.48	7.35	5.99	4.56	3.18	1.94	0.951
16	20.25	7.86	6.62	5.16	3.69	2.33	1.21	0.443
17	22.25	5.74	4.6	3.3	2.07	1.05	0.328	
18	24.25	4.19	3.12	1.98	1.01	0.315		
19	26.25	2.78	1.84	0.937	0.285			
20	28.25	1.61	0.863	0.259				
21	30.25	0.744	0.25					
22	32.25	0.197						

*It is the distance from the root of the blade to center of corresponding portion in meters.

Stress in Compression:

Table B.8: Data for Longitudinal Stress in compression (W+D)

Portion	Location*	Blade 1	Blade 2	Blade 3	Blade 4	Blade 5	Blade 6	Blade 7
1	0.35	11.4	11	10.6	9.98	9.32	8.6	7.8
2	1.2	11.2	10.8	10.3	9.69	8.99	8.23	7.4
3	2.2	12	11.6	11	10.3	9.49	8.62	7.68
4	3.2	13.5	12.9	12.2	11.4	10.4	9.4	8.3
5	4.2	15.3	14.6	13.7	12.7	11.6	10.4	9.06
6	5.2	18	17.1	16	14.7	13.3	11.7	10.1
7	6.2	25.4	24	22.2	20.2	18	15.5	13
8	6.85	36.3	34.4	31.9	29	25.9	22.4	18.9
9	7.625	28.2	26.6	24.6	22.2	19.6	16.8	13.9
10	8.75	25.7	24.1	22.1	19.8	17.3	14.6	11.8
11	10.25	18.7	17.4	15.8	14	12	9.96	7.86
12	12.25	15.2	14	12.5	10.8	8.98	7.13	5.31
13	14.25	14	12.7	11	9.21	7.32	5.44	3.68
14	16.25	9.17	8.18	6.97	5.67	4.34	3.06	1.92
15	18.25	7.15	6.21	5.06	3.87	2.71	1.67	0.836
16	20.25	8.7	7.33	5.72	4.09	2.59	1.34	0.477
17	22.25	5.44	4.33	3.07	1.9	0.977	0.318	
18	24.25	3.99	2.94	1.82	0.9	0.285		
19	26.25	2.63	1.71	0.844	0.265			
20	28.25	1.51	0.789	0.246				
21	30.25	0.662	0.223					
22	32.25	0.178						

*It is the distance from the root of the blade to center of corresponding portion in meters.

3. **Transverse Stress**

Stress in Tension:

Table B.9: Data for Transverse Stress in tension (W+D)

Portion	Location	Blade 1	Blade 2	Blade 3	Blade 4	Blade 5	Blade 6	Blade 7
1	0.35	0.366	0.358	0.348	0.336	0.321	0.305	0.286
2	1.2	0.345	0.331	0.316	0.297	0.277	0.254	0.25
3	2.2	0.571	0.549	0.52	0.486	0.449	0.407	0.362
4	3.2	0.707	0.667	0.616	0.574	0.527	0.475	0.419
5	4.2	0.833	0.786	0.734	0.674	0.608	0.543	0.474
6	5.2	1.08	1.02	0.949	0.867	0.775	0.676	0.583
7	6.2	1.54	1.46	1.35	1.23	1.09	0.948	0.795
8	6.85	2.57	2.44	2.27	2.07	1.85	1.61	1.37
9	7.625	3.66	3.53	3.35	3.14	2.91	2.64	2.34
10	8.75	4.1	3.93	3.71	3.45	3.15	2.82	2.46
11	10.25	4.7	4.47	4.17	3.82	3.43	3	2.55
12	12.25	3.12	2.96	2.75	2.51	2.25	1.95	1.63
13	14.25	2.47	2.33	2.14	1.92	1.68	1.42	1.13
14	16.25	2.06	1.91	1.73	1.51	1.27	1.02	0.754
15	18.25	1.78	1.62	1.42	1.19	0.947	0.692	0.444
16	20.25	1.82	1.6	1.33	1.04	0.748	0.467	0.243
17	22.25	1.38	1.19	0.96	0.708	0.457	0.245	
18	24.25	1.12	0.92	0.681	0.439	0.233		
19	26.25	0.827	0.63	0.402	0.207			
20	28.25	0.567	0.377	0.19				
21	30.25	0.33	0.175					
22	32.25	0.138						

*It is the distance from the root of the blade to center of corresponding portion

Stress in Compression:

Table B.10: Data for Transverse Stress in compression (W+D)

Portion	Location*	Blade 1	Blade 2	Blade 3	Blade 4	Blade 5	Blade 6	Blade 7
1	0.35	0.0837	0.0864	0.0897	0.0932	0.0967	0.101	0.109
2	1.2	0.231	0.211	0.185	0.156	0.124	0.09	0.0549
3	2.2	0.396	0.371	0.338	0.302	0.261	0.217	0.172
4	3.2	0.473	0.447	0.414	0.375	0.332	0.286	0.237
5	4.2	0.651	0.605	0.547	0.501	0.45	0.395	0.336
6	5.2	0.984	0.918	0.831	0.734	0.627	0.514	0.398
7	6.2	1.79	1.68	1.54	1.38	1.2	1.02	0.821
8	6.85	4.42	4.23	3.98	3.69	3.36	2.99	2.6
9	7.625	2.46	2.38	2.27	2.14	1.99	1.82	1.62
10	8.75	4.23	4.02	3.76	3.45	3.1	2.72	2.31
11	10.25	2.91	2.77	2.59	2.38	2.14	1.87	1.58
12	12.25	2.3	2.17	2.01	1.82	1.6	1.37	1.12
13	14.25	1.94	1.81	1.64	1.45	1.23	1	0.763
14	16.25	1.62	1.48	1.31	1.11	0.902	0.679	0.456
15	18.25	1.41	1.27	1.09	0.889	0.673	0.449	0.267
16	20.25	1.31	1.15	0.948	0.725	0.49	0.291	0.198
17	22.25	1.12	0.947	0.729	0.497	0.3	0.211	
18	24.25	0.871	0.693	0.472	0.279	0.202		
19	26.25	0.641	0.457	0.267	0.179			
20	28.25	0.409	0.254	0.164				
21	30.25	0.204	0.154					
22	32.25	0.1						

*It is the distance from the root of the blade to center of corresponding portion